JRC Scientific and Technical Reports

Assessment of thermal fatigue crack growth in the high cycle domain under sinusoidal thermal loading

An application – Civaux 1 case

V. Radu E. Paffumi N. Taylor K.-F. Nilsson

EUR 23223 EN - 2007

JRC
EUROPEAN COMMISSION

ie
Institute for Energy

The Institute for Energy provides scientific and technical support for the conception, development, implementation and monitoring of community policies related to energy. Special emphasis is given to the security of energy supply and to sustainable and safe energy production.

European Commission
Joint Research Centre
Institute for Energy

Contact information
Address: N. Taylor
E-mail: Nigel.taylor@ec.europa.eu
Tel.: +31-224-565202
Fax: +31-224-565641

http://ie.jrc.ec.europa.eu
http://www.jrc.ec.europa.eu

JRC 41641

EU 23223 EN
ISSN 1018-5593

ISBN : 978-92-79-08218-4
DOI : 10.2790/4943

Luxembourg: Office for Official Publications of the European Communities

Printed in The Netherlands

Assessment of thermal fatigue crack growth in the high cycle domain under sinusoidal thermal loading

An application – Civaux 1 case

V. Radu E. Paffumi N. Taylor K.-F. Nilsson

CONTENTS

Abstract

The assessment of fatigue crack growth due to cyclic thermal loads arising from turbulent mixing presents significant challenges, principally due to the difficulty of establishing the actual loading spectrum. So-called sinusoidal methods represents a simplified approach in which the entire spectrum is replaced by a sine-wave variation of the temperature at the inner pipe surface. The amplitude can be conservatively estimated from the nominal temperature difference between the two flows which are mixing; however a critical frequency value must be determined numerically so as to achieve a minimum predicted life. The need for multiple calculations in this process has lead to the development of analytical solutions for thermal stresses in a pipe subject to sinusoidal thermal loading, described in a companion report.

Based on these stress distributions solutions, the present report presents a methodology for assessment of thermal fatigue crack growth life. The critical sine wave frequency is calculated for both axial and hoop stress components as the value that produces the maximum tensile stress component at the inner surface. Using these through-wall stress distributions, the corresponding stress intensity factors for a long axial crack and a fully circumferential crack are calculated for a range of crack depths using handbook K solutions. By substituting these in a Paris law and integrating, a conservative estimate of thermal fatigue crack growth life is obtained. The application of the method is described for the pipe geometry and loadings conditions reported for the Civaux 1 case. Additionally, finite element analyses were used to check the thermal stress profiles and the stress intensity factors derived from the analytical model. The resulting predictions of crack growth life are comparable with those reported in the literature from more detailed analyses and are lower bound, as would be expected given the conservative assumptions made in the model.

Nomenclature

a - crack depth
l - wall-thickness of the pipe
r_i , r_o - inner and outer radii of the pipe
θ - temperature change from the reference temperature
T_o - reference temperature
r - radial distance
k - thermal diffusivity
λ - thermal conductivity
ρ - density
c - specific heat coefficient
F(t) - function of time representing the thermal boundary condition applied on the inner surface of the cylinder
$J_\upsilon(z)$, $Y_\upsilon(z)$ - Bessel functions of first and second kind of order υ
θ_0 - amplitude of temperature wave
ω - wave frequency in rad/s
f - wave frequency in Hz
t - time variable
s_n - positive roots of the transcendental equation (kernel of finite Hankel transform)
ε_r - radial strain
ε_θ - hoop strain
ε_z - axial strain
σ_r - radial stress
σ_θ - hoop stress
σ_z - axial stress
x - radial local coordinate originating at the internal surface of the component
σ_0 -uniform coefficient for polynomial stress distribution
σ_1 -linear coefficient for polynomial stress distribution

σ_2 -quadratic coefficient for polynomial stress distribution

σ_3 -third order coefficient for polynomial stress distribution

σ_4 -fourth order coefficient for polynomial stress distribution

E - Young's modulus

α - coefficient of the linear thermal expansion

v - Poisson's ratio

u - radial displacement

$\frac{da}{dN}$ - increment of crack growth for a given cycle

C - fatigue crack growth law parameter

n - fatigue crack growth law exponent

$\Delta K_{max}=K_{max}- K_{min}$ - maximum stress intensity factor range

K_{max} - maximum stress intensity factor

K_{min} - minimum stress intensity factor

ΔK_{th} - the threshold stress intensity factor range

$\Delta K_{eff} = \frac{\Delta K}{(1-R)^m}$ - effective stress intensity range

$R = \frac{K_{\min}}{K_{\max}}$ - stress intensity factor ratio

m - parameter in the ΔK_{eff} expression

σ_{VM} - effective stress range intensity (Von Mises equivalent stress)

ΔS_{range} - effective equivalent stress range intensity

G_0, G_1, G_2, G_3, G_4 - the influence coefficients of hoop stress distribution

$G'_0, G'_1, G'_2, G'_3, G'_4$ - the influence coefficients of axial stress distribution

K_{Iaxial} - the Mode I stress intensity factor for an infinite longitudinal surface crack

K_{Icirc} - the Mode I stress intensity factor for a fully circumferential surface crack

1. Introduction

Quantifying the thermal fatigue damage and subsequent crack growth which may arise due to thermal stresses from turbulent mixing or vortices in light water reactor (LWR) piping systems remains a demanding task and much effort continues to be devoted to experimental, FEA and analytical studies [1, 2, 3, 4].

The problem of thermal fatigue in mixing areas arises in pipes where a turbulent mixing or vortices produce rapid fluid temperature fluctuations with random frequencies. The results in temperature fluctuations can be local or global and induce random variations of local temperature gradients in structural walls of pipe, which lead to cyclic thermal stresses [5, 6]. These cyclic thermal stresses are caused by oscillations of fluid temperature and the strain variations result in fatigue damage, cracking and crack growth.

The response of structures to thermal loads depend on the heat transfer process. In certain components the pipe wall does not respond to high frequency fluctuation of fluid temperature because of heat transfer loss, and low frequency components of fluctuation may not cause large thermal stresses because of thermal homogenization [7,8]. Numerical simulations of the type of thermal stripping[1] and high-cycle thermal fatigue that can occur at tee junctions of LWR piping systems have shown that the critical oscillation frequency of surface temperature is the range 0.1-1 Hz [5, 6, 9, 10, 11].

In a previous work [12] an analytical set of solutions was developed for thermal stresses in a hollow cylinder subject to sinusoidal thermal loading based on the Hankel transform, properties of Bessel's functions and the thermoelasticity governing equations. The solution of the time-dependence of temperature in a hollow cylinder allows the derivation of analytical solutions for the associated thermal stresses and their profiles through the wall-thickness.

[1] Thermal striping is defined as effect of a rapid random oscillation of the surface temperature inducing a corresponding fluctuation of surface stresses and strains in adjacent metal.

In the present paper, the Civaux 1 case [1] was used to assess the application of these analytical thermal stress solutions in crack growth life assessment in the high cycle thermal fatigue domain. The time-dependent analytical solution for thermal stresses in pipe components were used to analyze critical frequencies for axial and hoop stresses as well as for von Mises equivalent stress intensities. Each critical frequency has been derived based on the maximum range of thermal stresses. The maximum stress intensity factor range ΔK_I^{max} is considered for two types of crack: a long axial crack and fully circumferential crack on inner surface of the pipe. The fatigue crack growth approach is based on the stress intensity factor solutions expressed in terms of a fourth order polynomial stress distribution through thickness. The crack growth analyses use a Paris-law type equation. Finally, the predictions are compared with the results of other analyses of the Civaux case reported in the literature.

Figure 1 shows a flow-chart which describes the steps performed for analysis of thermal fatigue crack growth due to sinusoidal thermal loading.

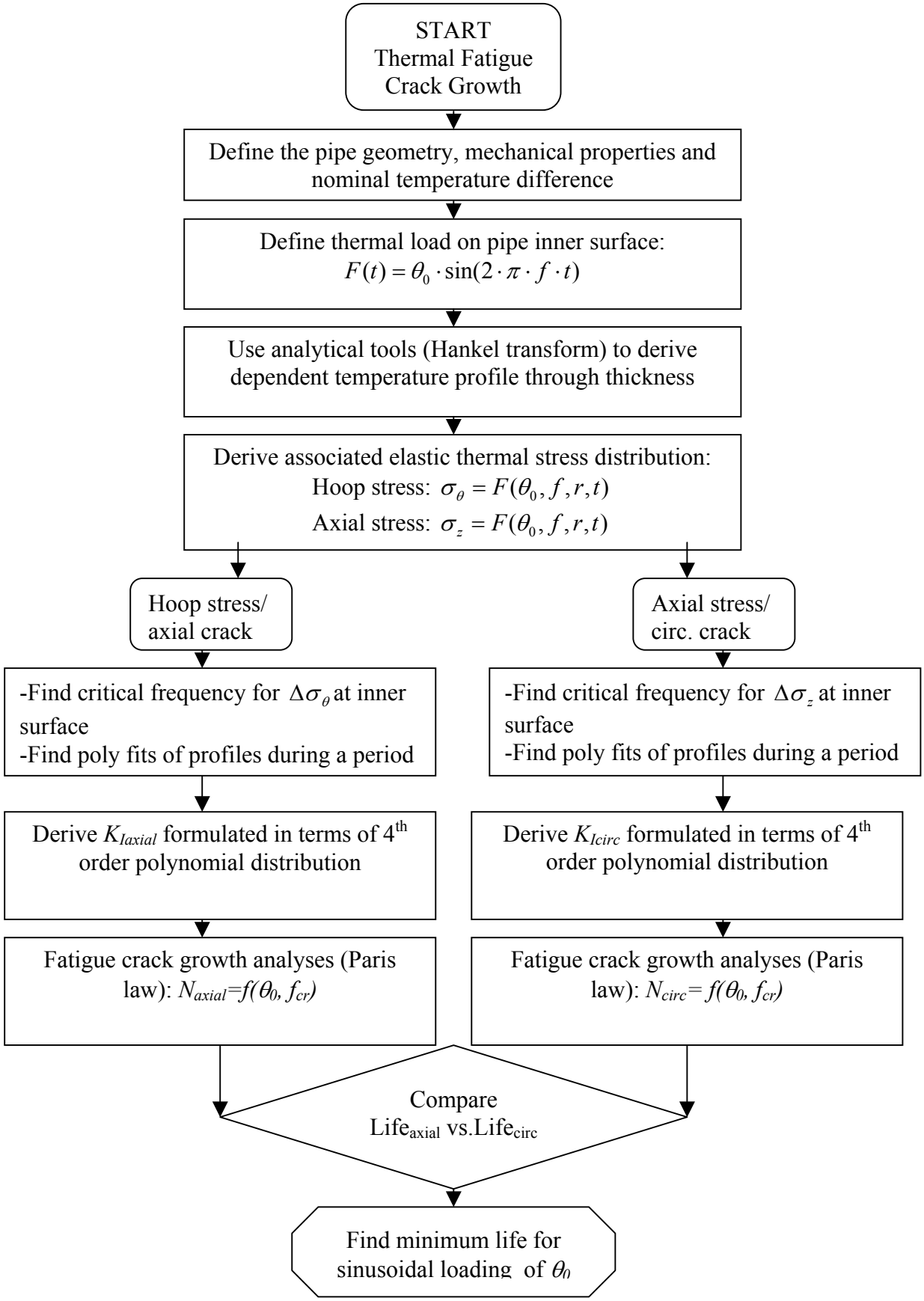
START
Thermal Fatigue
Crack Growth
Define the pipe geometry, mechanical properties and nominal temperature difference
Define thermal load on pipe inner surface:
$F(t) = \theta_0 \cdot \sin(2 \cdot \pi \cdot f \cdot t)$
Use analytical tools (Hankel transform) to derive dependent temperature profile through thickness
Derive associated elastic thermal stress distribution:
Hoop stress: $\sigma_\theta = F(\theta_0, f, r, t)$
Axial stress: $\sigma_z = F(\theta_0, f, r, t)$
Hoop stress/ axial crack
Axial stress/ circ. crack
-Find critical frequency for $\Delta\sigma_\theta$ at inner surface
-Find poly fits of profiles during a period
-Find critical frequency for $\Delta\sigma_z$ at inner surface
-Find poly fits of profiles during a period
Derive K_{Iaxial} formulated in terms of 4th order polynomial distribution
Derive K_{Icirc} formulated in terms of 4th order polynomial distribution
Fatigue crack growth analyses (Paris law): $N_{axial}=f(\theta_0, f_{cr})$
Fatigue crack growth analyses (Paris law): $N_{circ}= f(\theta_0, f_{cr})$
Compare
$Life_{axial}$ vs.$Life_{circ}$
Find minimum life for sinusoidal loading of θ_0

Figure 1. Flow–chart for assessment of thermal fatigue crack growth life under sinusoidal thermal loading

2. Thermal stresses developed under sinusoidal thermal loading in pipes

The thermal stresses in a LWR piping subsystem are dependent on the temperature distribution arising from the various operation conditions. It should be noted that the assessment of temperature fields is easier to perform for a pipe than for components with complex geometries: a pipe can be represented as a hollow cylinder and for such a simple geometry it becomes possible to use analytical tools to get the time-dependent temperature profile through wall thickness. In a previous work [12] analytical solutions were developed for temperature fields and associated elastic thermal stress distributions for a hollow cylinder subject to sinusoidal transient thermal loading. Since these form the bases of the fatigue crack growth method presented in this report, some of the main features will be summarized in the following.

A hollow cylinder, made of a homogeneous isotropic material with inner and outer radii r_i *and* r_o respectively is assumed. The one-dimensional heat diffusion equation in cylindrical coordinates and with axisymmetric thermal variations is [8, 13, 14]:

$$\frac{\partial^2\theta}{\partial r^2}+\frac{1}{r}\cdot\frac{\partial\theta}{\partial r}=\frac{1}{k}\cdot\frac{\partial\theta}{\partial t} \tag{1}$$

Here $\theta = T(r,t) - T_o$ (2)

is the change in temperature from the reference temperature, T_o, which is the temperature of the body in the unstrained state or the ambient temperature before changing of temperature.

Other parameters in Equation (1) are:

r - radial distance;

k - the thermal diffusivity which is defined as:

$$k=\frac{\lambda}{\rho c} \tag{3}$$

λ – the thermal conductivity;

ρ - the mass density;

c – the specific heat coefficient;

The thermal boundary conditions (Dirichlet conditions) for a hollow cylinder were considered as follow:

- inner surface thermal loading

$$\theta(r_i,t) = F(t) \tag{4}$$

- outer surface (adiabatic condition hypothesis)

$$\theta(r_o,t) = 0 \tag{5}$$

The initial condition for the through wall-thickness temperature was considered as

$$\theta(r,0) = 0 \tag{6}$$

In Equation (4) the thermal loading given by function *F(t)* is a known function of time representing the thermal boundary condition applied on the inner surface of the cylinder. The sinusoidal thermal loading boundary condition is expressed as

$$F(t) = \theta_0 \cdot \sin(\omega \cdot t) = \theta_0 \cdot \sin(2\pi \cdot f \cdot t) \tag{7}$$

where

θ_0 – amplitude of temperature wave;

ω , *f* - the wave frequency in rad/s and cycles/sec, respectively;

t – time variable.

By means of Hankel transform methodology [15, 16, 17] and using some properties of Bessel functions, the solution for temperature distribution during a thermal transient for a hollow cylinder can be written as follows [12]:

$$\theta(r,t) = k \cdot \pi \cdot \sum_{n=1}^{\infty} \theta_1(r_i, r_o, s_n) \cdot \theta_2(r_i, r, s_n) \cdot \theta_3(t, s_n) \tag{8}$$

where

$$\theta_1(r_i, r_o, s_n) = \frac{s_n^2 \cdot J_0^2(s_n \cdot r_o)}{J_0^2(s_n \cdot r_o) - J_0^2(s_n \cdot r_i)} \tag{9}$$

$$\theta_2(r_i, r, s_n) = Y_o(s_n \cdot r_i) \cdot J_o(s_n \cdot r) - J_o(s_n \cdot r_i) \cdot Y_o(s_n \cdot r) \tag{10}$$

$$\theta_3(t, s_n) = e^{-k \cdot s_n^2 \cdot t} \int_0^t e^{k \cdot s_n^2 \cdot \tau} F(\tau) d\tau \tag{11}$$

By substituting Equation 7 into Equation 11 and integrating are obtains:

$$\theta_3(\omega, t, s_n) = \theta_0 \cdot \frac{\omega \cdot e^{-k \cdot s_n^2 \cdot t} + (k \cdot s_n^2) \cdot \sin(\omega \cdot t) - \omega \cdot \cos(\omega \cdot t)}{(k \cdot s_n^2)^2 + \omega^2} \tag{12}$$

Thus the complete formula for temperature distribution through wall-thickness of hollow circular cylinder in case of sinusoidal thermal loading is given by:

$$\theta(r,\omega,t) = k\cdot\pi\cdot\sum_{n=1}^{\infty}\frac{s_n^2\cdot J_0^2(s_n\cdot r_o)}{J_0^2(s_n\cdot r_o)-J_0^2(s_n\cdot r_i)}\left[Y_o(s_n\cdot r_i)\cdot J_o(s_n\cdot r)-J_o(s_n\cdot r_i)\cdot Y_o(s_n\cdot r)\right]\times$$
$$\times\left[\theta_0\cdot\frac{\omega\cdot e^{-k\cdot s_n^2\cdot t}+(k\cdot s_n^2)\cdot\sin(\omega\cdot t)-\omega\cdot\cos(\omega\cdot t)}{(k\cdot s_n^2)^2+\omega^2}\right] \quad (13)$$

where s_n are the positive roots of the transcendental equation

$$Y_o(s_n\cdot r_i)\cdot J_o(s_n\cdot r_o)-J_o(s_n\cdot r_i)\cdot Y_o(s_n\cdot r_o)=0 \quad (14)$$

Equation (13) shows that the temperature distribution is radial and it has been used in the general solution for thermal stress components.

For thermal stress evaluation we assumed that the thermo-mechanical properties are the same as during the thermal transient analyses.

The one-dimensional equilibrium equation in the radial direction for a hollow cylinder is [13, 14]:

$$\frac{d\sigma_r}{dr}+\frac{\sigma_r-\sigma_\theta}{r}=0 \quad (15)$$

where σ_r and σ_θ are the radial and hoop stress respectively. In the axisymmetric problem with small strains, the strain-displacement relations are:

$$\varepsilon_r=\frac{du}{dr} \quad (16)$$

$$\varepsilon_\theta=\frac{u}{r} \quad (17)$$

$$\varepsilon_{r\theta}=0 \quad (18)$$

where u is the radial displacement.

The displacement technique has been used to solve the axisymmetric problems of hollow cylinder. The components of stress in cylindrical coordinates can be expressed as

$$\sigma_r=\frac{E'}{1-\nu'^2}\left[\frac{du}{dr}+\nu'\cdot\frac{u}{r}-(1+\nu')\cdot\alpha'\cdot\theta+(1+\nu')\cdot c'\right] \quad (19)$$

$$\sigma_\theta=\frac{E'}{1-\nu'^2}\left[\nu'\cdot\frac{du}{dr}+\frac{u}{r}-(1+\nu')\cdot\alpha'\cdot\theta+(1+\nu')\cdot c'\right] \quad (20)$$

$$\sigma_{r\theta}=0 \quad (21)$$

In the case of plane strain and plane stress, the meanings of the constants from Equations (19) and (20) are:

$$E' = \begin{cases} \dfrac{E}{1-\nu^2} \\ E \end{cases}$$ E –Young modulus (22)

$$\nu' = \begin{cases} \dfrac{\nu}{1-\nu} \\ \nu \end{cases}$$ ν - Poisson's ratio (23)

$$\alpha' = \begin{cases} (1+\nu)\alpha \\ \alpha \end{cases}$$ α -coefficient of the linear thermal expansion (24)

$$c' = \begin{cases} \nu\varepsilon_0 \\ 0 \end{cases}$$ ε_0 – constant axial strain for plain strain state (25)

The substitution of Equations (19, 20) in Equation 15 yields

$$\frac{d}{dr}\left[\frac{1}{r}\cdot\frac{d(r\cdot u)}{dr}\right] = (1+\nu')\cdot\alpha'\cdot\frac{d\theta(r,t)}{dr} \tag{26}$$

The general solution of Eq. (26) is

$$u = (1+\nu')\cdot\alpha'\cdot\frac{1}{r}\int_r \theta(r,t)\cdot r\cdot dr + C_1\cdot r + \frac{C_2}{r} \tag{27}$$

The integration constants C_1 and C_2 may be determined from the boundary conditions. The radial stress component is negligible for thin-walled cylinder compared to the hoop and axial stress components. The hoop and axial stress components are given in the following relationships in the case of plane strain [12]:

$$\sigma_\theta(r,\omega,t) = \frac{\alpha\cdot E}{1-\nu}\left[\frac{1}{r^2}\cdot I_1(r,\omega,t) + \frac{r^2+r_i^2}{r^2\cdot(r_o^2-r_i^2)}\cdot I_2(\omega,t) - \theta(r,\omega,t)\right] \tag{28}$$

$$\sigma_z(r,\omega,t) = \frac{\alpha\cdot E}{1-\nu}\left(\frac{2\nu}{r_o^2-r_i^2}\cdot I_2(\omega,t) - \theta(r,\omega,t)\right) \quad \text{for } \varepsilon_z=0 \tag{29}$$

$$\sigma_z(r,\omega,t) = \frac{\alpha\cdot E}{1-\nu}\left(\frac{2}{r_0^2-r_i^2}\cdot I_2(\omega,t) - \theta(r,\omega,t)\right) \quad \text{for } \varepsilon_z=\varepsilon_0 \tag{30}$$

The mathematical relationships for $I_1(r,\omega,t)$ and $I_2(\omega,t)$ with the complete equations for both thermal stress components are given in Appendix 1.

The case with fixed boundary condition (ε_z=0) in axial direction of hollow cylinder gives a higher level of maximum axial thermal stress than when the end of the cylinder is free

to extend ($\varepsilon_z=\varepsilon_0$ case). The predictions from the above equations for thermal stress were checked with those of finite element analyses performed with the ABAQUS computer code [12], with satisfactory results.

3. Thermal fatigue crack growth approach

Crack growth by fatigue arises from varying loads on the component, resulting in cyclic stresses in the crack tip region. The crack tip stress intensity factor is a very useful parameter for predicting crack growth behavior as long as the behavior of the material bulk is elastic and plastic deformation is limited to a small region at the crack tip. Linear elastic fracture mechanics (LEFM) has been validated to correlate the increment of crack growth per cycle to the applied stress intensity range through a fatigue crack growth law. In using fracture mechanics to describe fatigue crack growth the minimum value of the stress intensity factor in a cycle is usually taken to be zero (K_{min} =0) when stress intensity factor ratio, $R = \frac{K_{\min}}{K_{\max}} \le 0$ [18]. The rate of the crack growth, *da/dN* , in terms of the crack tip stress intensity factor range, ΔK, can be written as:

$$\frac{da}{dN} = f(\Delta K) \tag{31}$$

The equations commonly used to describe the function $f(\Delta K)$ are based on the trends developed by experimental data. Numerous fatigue crack growth rate empirical and analytical relationships have been developed (see [18] for instance).

Generally speaking, three regimes (I, II and III) are associated with fatigue crack growth (Figure 2). For region I (or fatigue regime A), the crack growth rate *(da/dN)* is low and the corresponding stress intensity range, ΔK, approaches a minimum value called the threshold intensity factor, ΔK_{th} , below which the crack does not grow. For region III (or fatigue regime C), the crack growth is rapid and accelerates until the crack tip stress intensity factor reaches its critical value. For region II (or fatigue regime B) the simplest and most common form of the fatigue crack growth law is the Paris law. It is applicable only in the middle region of crack growth curve, where the variation of *log(da/dN)* with respect to *log* (ΔK) is linear.

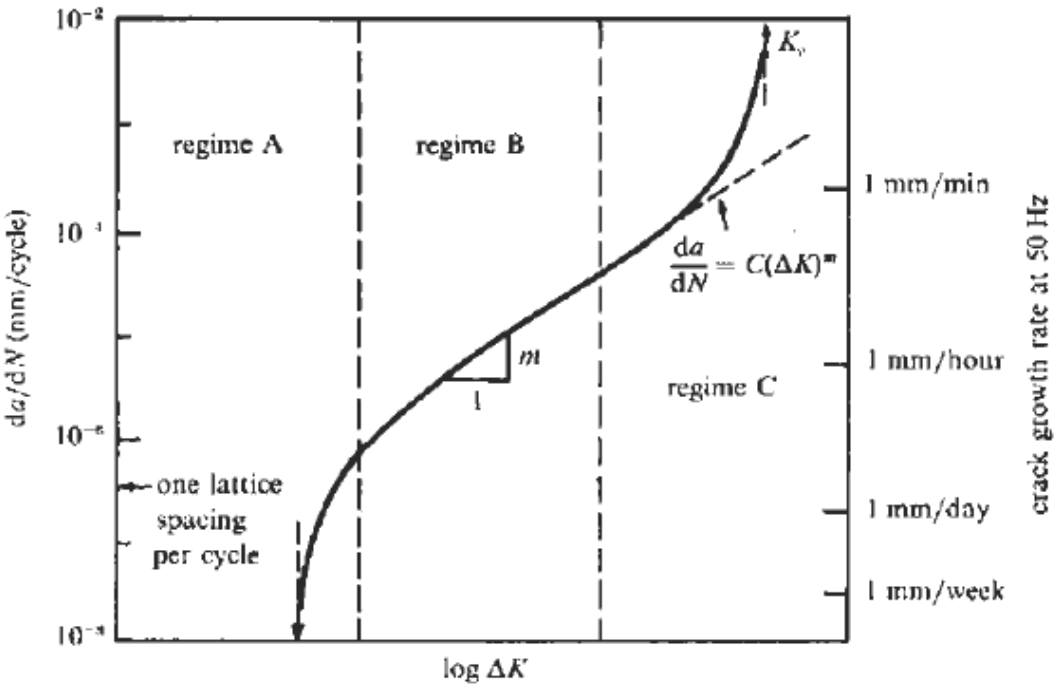

Figure 2. Fatigue crack growth regimes [18]

In this model the crack growth rate is independent of the stress ratio:

$$\frac{da}{dN} = C.(\Delta K)^n \tag{32}$$

where,

$\frac{da}{dN}$ - increment of crack growth for a given cycle,

C - scaling parameter,

n - exponent

ΔK $=K_{max}- K_{min}$, stress intensity factor range; if $\Delta K>\Delta K_{th}$ the crack will grow, otherwise the crack growth does not occur i.e. $\frac{da}{dN}=0$;

K_{max} - maximum stress intensity factor for a given cycle,

K_{min} - minimum stress intensity factor for a given cycle,

ΔK_{th} - the threshold stress intensity factor range.

To use the Paris crack growth relation described by Equation (32) beyond its validity limit can result in life estimation error. A generalization of the Paris law is the Walker equation, which is also simple and has the form:

$$\frac{da}{dN} = C.\left(\Delta K_{eff}\right)^n \tag{33}$$

where

$$\Delta K_{eff} = \frac{\Delta K}{\left(1-R\right)^m} \quad \text{- effective stress intensity factor range,} \tag{34}$$

$$R = \frac{K_{\min}}{K_{\max}} \quad \text{- stress intensity factor ratio,} \tag{35}$$

m - material parameter.

More advanced forms of fatigue crack growth laws that accounting for factors such as stress ratio, ranges of ΔK, effects of a threshold stress intensity factor ΔK_{th} and plasticity-induced crack closure are available for many materials and operational environments.

An empirical equation describing the crack growth behaviour in regimes B and C, including the effect of *R* is Foreman equation:

$$\frac{da}{dN} = \frac{C \cdot \left(\Delta K\right)^n}{\left(1-R\right)K_c - \Delta K} \tag{36}$$

C - material parameter,

n - material parameter,

K_c - the fracture toughness of material, thickness dependent.

Equation (36) was later modified by Forman-Newman-de Koning (FNK) [18] to account for all regions of the crack growth curve, including the stress ratio and crack closure effects:

$$\frac{da}{dN} = \frac{C\left(1-f\right)^n \cdot \left(\Delta K\right)^n \cdot \left(1-\frac{\Delta K_{th}}{\Delta K}\right)^p}{\left(1-R\right)^n \left(1-\frac{\Delta K}{\left(1-R\right)K_c}\right)^q} \tag{37}$$

C,n,p,q - empirical derived constants;

R - stress ratio;

ΔK - stress intensity factor range;

ΔK_{th} - the threshold stress intensity factor range

In order to perform comparison of the present results with those of reference [1], the crack growth life assessment in the present work was determined applying Equation (33), where the constants *C* and *n* are known and the effective stress intensity range is specified as:

$$\Delta K_{eff} = q(R).\Delta K_I \tag{38}$$

Recommendations from reference [1] are the following:

if *R<0* , then $$q(R) = \frac{1-0.5.R}{1-R} \tag{39}$$

and if *R>0* $$q(R) = \frac{1}{1-0.5R} \tag{40}$$

Two types of cracks with constant depth were considered on the inner surface of the pipe:

- infinite long axial crack in radial-axial plane;
- fully circumferential crack in radial-transverse plane.

The stress distribution through wall-thickness used for the stress intensity factor assessment is based on the component of stress normal to the crack face. Therefore, for the state of stress at the location of a crack we consider elastic thermal stresses given by analytical solutions for hoop stress in first crack type, and axial stress *(*with ε_z*=0*) for the second one.

4. Fatigue life associated with the critical frequencies for thermal stress ranges (Civaux 1 case)

4.1. Description of the Civaux 1 case

The methodology described in the following paragraphs considers crack growth life assessment in a thermal fatigue application. It is based on the analytical solutions obtained for elastic thermal stresses due to sinusoidal thermal loading on inner surface of a hollow cylinder and is applied to the leak event which occurred on the Civaux 1 plant. The main characteristics of the piping system from Civaux 1 case have been described in [1]. Some of features concerning on this thermal fatigue damaging case are given in the following.

In 1998 a longitudinal crack was discovered at outer edge of an elbow in a mixing zone of the Residual Heat Removal System (RHRS) of the Civaux NPP unit 1 [1]. An extensive investigation was carried out and the conclusion was that the origin of this degradation phenomenon was cracking by thermal fatigue. The incident was caused by fluctuations in the temperature of the fluid downstream mixing tee. It is worth mentioning that the time between initiation of the crack and its development to a significant depth through the wall was only about ≈1500 hours, which is surprisingly low.

Metallurgical examinations revealed substantial cracks and also some networks of small thermal fatigue cracks in the vicinity of the welds, but no fabrication defects. The section of interest is shown in Figure 3. The system operated at a pressure of 36 bar, the hot leg contains water at 180° C and the cold leg contains water at 20°C. In the damage zone of interest the pipe inner radius was $r_i \cong 120$ mm and outer radius was $r_o = 129$ mm. The material properties are shown in Table 1.

Table 1 Thermal and mechanical properties of austenitic steel (304L) at room temperature [1]

$c\left[\frac{J}{kg \cdot C}\right]$	$\lambda\left[\frac{W}{m \cdot C}\right]$	$\rho\left[\frac{kg}{m^3}\right]$	$\alpha\left[\frac{1}{C}\right]$	$E\left[\frac{N}{m^2}\right]$	v	$k\left[\frac{m^2}{s}\right]$
480	14.7	7800	$16.4.10^{-6}$	177.10^{9}	0.3	3.93×10^{-6}

c - specific heat coefficient, λ - thermal conductivity, ρ - density, α - mean thermal expansion, k – thermal diffusivity coefficient.

The temperature fluctuation was reported to be in the range 20-180° C and on the inner surface of the pipe the maximum temperature fluctuation range was estimated to be 120°C [1].

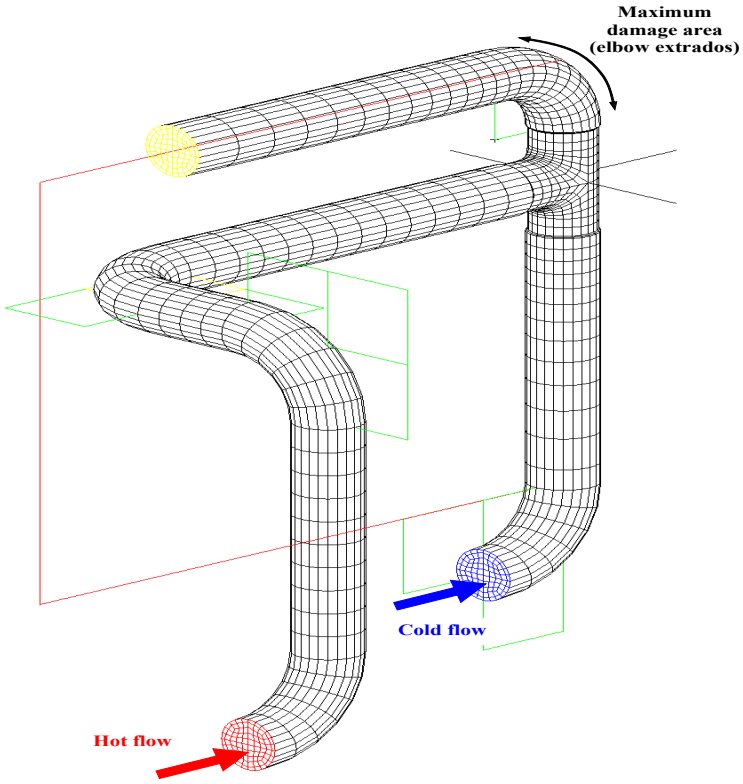

Figure 3. The simplified sketch of piping subsystems with damaged area by thermal fatigue cracking [1]

Analytical solutions for thermal stress components have been developed assuming a sinusoidal form of the thermal loading on the pipe inner surface. Therefore, the function applied as the inner thermal boundary condition, Equation (7), is

$$F(t) = \theta_0 \cdot \sin(\omega t) \tag{41}$$

For a maximum temperature range fluctuation of 120° C, as mentioned above, the temperature wave amplitude was set up to θ_0 =60°C:

$$F(t) = 60 \cdot \sin(2 \cdot \pi \cdot f \cdot t) \tag{41'}$$

4.2 The stress intensity factors for internal surface cracks in pipe for a highly nonlinear stress distribution

Fatigue cracks in piping components that develop due to fluctuation of thermal conditions are subjected to the thermal stresses which are usually highly nonuniform through wall-thickness. In many cases the available handbook stress intensity factors solutions are suitable for a direct crack growth assessment. For cracks in complex

stress fields such as residual or thermal stresses two methods are mostly used to calculate stress intensity factors:

- the weight function method
- stress intensity factor solutions formulated in terms of a fourth order polynomial stress distribution.

The weight function method has been used to compute the stress intensity factor for an arbitrary through-wall stress distribution in some references [19, 20, 21, 22, 23, 24]. The thermal transient stress problems of a hollow cylinder containing some kinds of cracks have been treated, mostly for the stress intensity factors in a cylinder containing a semielliptical surface crack subjected to stress gradients in the directions of depth [25, 26, 27, 28, 29, 30].

For a long axial crack and a fully circumferential crack our approach to derive the stress intensity factors are based on the polynomial representation of stress components through the wall-thickness of the pipe. The fourth order polynomial distribution can be used for highly non-linear stress distributions, such as the hoop and axial stresses arising during a period of sinusoidal thermal loading, by curve-fitting the analytical stress distribution.

The general form of the fourth order polynomial distribution is [31]:

$$\sigma(x) = \sigma_0 + \sigma_1\left(\frac{x}{l}\right) + \sigma_2\left(\frac{x}{l}\right)^2 + \sigma_3\left(\frac{x}{l}\right)^3 + \sigma_4\left(\frac{x}{l}\right)^4 \qquad (42)$$

where:

x – radial local coordinate originating at the internal surface of the component;

l – wall thickness;

σ_0 -uniform coefficient for polynomial stress distribution (MPa);

σ_1 -linear coefficient for polynomial stress distribution (MPa);

σ_2 -quadratic coefficient for polynomial stress distribution (MPa);

σ_3 -third order coefficient for polynomial stress distribution (MPa);

σ_4 -fourth order coefficient for polynomial stress distribution.

To evaluate the Mode I stress intensity factor, K_I, for surface crack under thermal stresses, the procedure from ref [31] was followed, which uses the following relation:

$$K_I(\frac{a}{l}) = \left[G_0\sigma_0 + G_1\sigma_1\left(\frac{a}{l}\right) + G_2\sigma_2\left(\frac{a}{l}\right)^2 + G_3\sigma_3\left(\frac{a}{l}\right)^3 + G_4\sigma_4\left(\frac{a}{l}\right)^4 \right]\sqrt{\frac{\pi a}{Q}} \quad (43)$$

where G_0, G_1, G_2, G_3, G_4 are the influence coefficients of the stress distribution. In the case of a long axial crack and also fully circumferential crack on inner pipe surface the Q parameter is considered as $Q=1$.

Usually, the influence coefficient values are provided in published tables as function of the component and crack geometry, also with certain geometric/dimensional limits. In ref. [31] these limits are

$$0.0 \le \frac{a}{l} \le 0.8 \quad (44)$$

$$2 \le \frac{r_i}{l} \le 1000 \quad (45)$$

where a- is the crack depth, l- is the wall thickness, r_i –is the inner radius

For the pipe geometry of the Civaux 1 case, the ratio in Equation (45) is:

$$\frac{r_i}{l} \approx 13\,. \quad (46)$$

In our assessment a cubic spline interpolating method has been applied on labeled data in order to provide the adequate influence coefficients G_0, G_1, G_2, G_3, G_4, for Civaux 1 case geometry.

4.3 Application on the Civaux 1 case

The analytical solutions for the temperature distribution and associated thermal stress components were implemented by means of specially written routines in the MATLAB software package (MATLAB 7.3 version, with the Symbolic Math Toolbox) [12]. Assessment of the thermal response under sinusoidal thermal loading on inner surface, given by Equation (13), needs the positive roots s_n of the transcendental Equation (14). The analytical solutions from Equations (28 to 30), which describe the associated elastic thermal stress components through wall – thickness, require also the positive roots of Equation (14). The analyses performed in a previous work [12], showed that using first one hundred positive roots provides a stable and optimized analytical response for stresses. For Civaux 1 case, where the geometry of the pipe consists in inner and outer

radii by r_i=0.1197m ≅ 0.120 m and r_o=0.129 m, the first 100 roots of transcendental Equation (14) are given in Appendix 2.

4.3.1 Critical frequencies for maximum stress ranges

In order to obtain the K_I dependence on crack depth versus time, during a thermal loading cycle, a first step is to define which frequency of loading spectra will be used for stress analysis. This frequency, which could be nominated as a “critical frequency”, is defined as the frequency at which the stress range is maximum (for hoop and axial stress or for effective stress range intensity).

A detailed analysis of critical frequencies was performed for hoop stress (Appendix 3). The analytical formula for hoop stress under sinusoidal thermal loading allows determination of the critical frequencies associated with geometric points through the wall-thickness. These critical frequencies are referred as *specific* critical frequencies corresponding to the maximum hoop stress range at selected points. The analysis looked at the distribution of specific critical frequencies in the radial direction from inner surface up to a depth of 6 mm (the wall-thickness is 9 mm) (see Appendix 3). Moving into the wall from the inner surface of the pipe the specific critical frequencies take values between 0.01Hz and 4.5 Hz. The dependence of maximum amplitudes of hoop stress on associated critical frequencies through thickness are shown in Figure 4. It compares the hoop stress profile for f_{cr}=0.3 Hz (associated with inner surface) with maximum hoop stress profile at specific critical frequencies for different geometric points through wall-thickness.

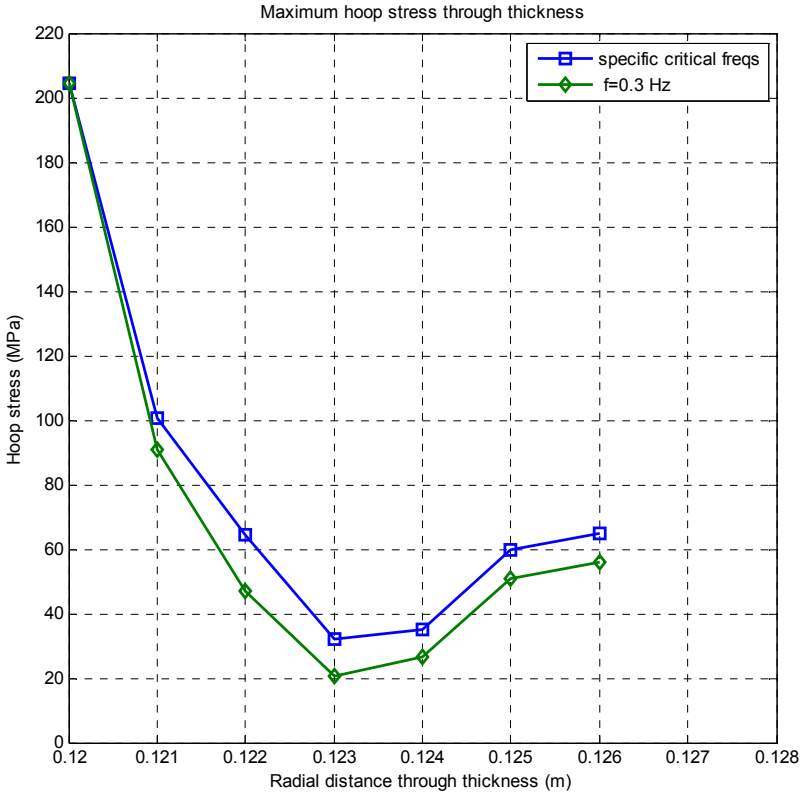

Figure 4. Comparison between maximum values of hoop stress at specific critical frequencies $f_{cr}spec$=0.09 - 4.5 Hz and the values at f_{cr}=0.3 Hz (critical frequency for maximum hoop stress on inner surface)

There are no significant differences between maximum hoop stress profiles derived from both approaches. On this basis for the crack growth analyses for an axial crack it is considered sufficient to use the profiles corresponding to the critical frequency valid for the inner surface. The same approach is used for axial stress, i.e. when arising circumferential cracks.

As already mentioned, for each set of boundary conditions there is a certain frequency (critical frequency), at which the component stresses range is maximum on inner surface. To find these critical frequencies for each thermal stress component we use the mathematical series expansion described by Equations 28, 29 and 30. In respect of this the frequency has been chosen as main variable, taking values in the range 0.01Hz - 10 Hz and the *r* variable (radial coordinate) was set up *r*= 0.120 m (≈ inner pipe radius value). Figure 5 shows the stress range dependencies on thermal loading frequencies, for hoop and axial stress components at the inner surface.

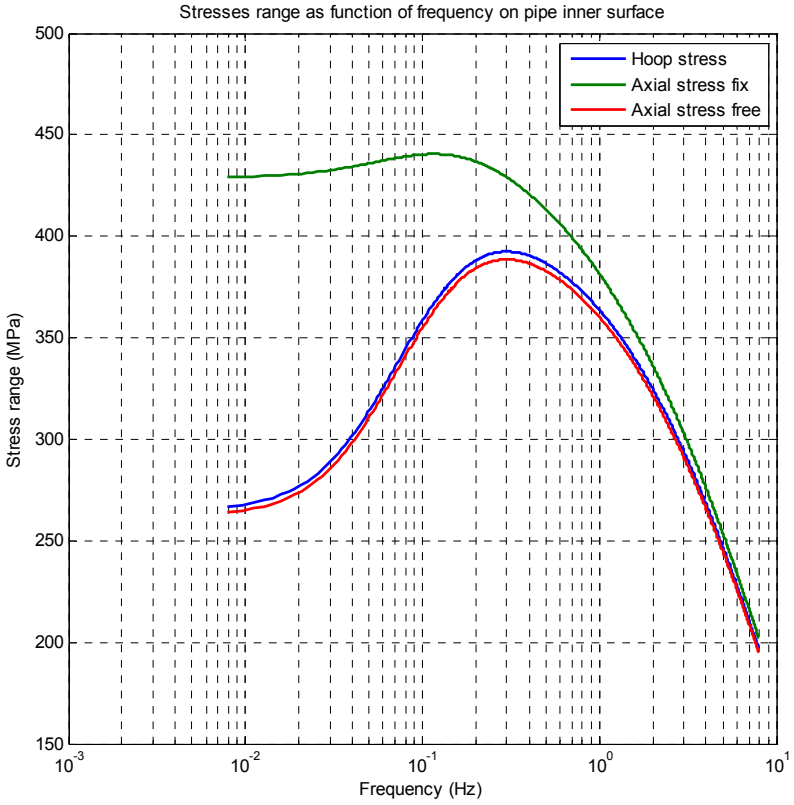

Figure 5. Dependence of maximum stress ranges on thermal loading frequencies (inner surface, Civaux 1 case)

The critical frequencies are listed in Table 2 with the corresponding stress range values.

Table 2 Critical frequencies for stress components in pipe under sinusoidal thermal loading

Stress components	Critical frequency f (Hz)	Stress Range $\Delta\sigma$ (MPa)	Notes/Comments
Hoop stress	0.3	392	
Axial stress	0.1	440	$\varepsilon_z=0$
Axial stress	0.3	388	$\varepsilon_z=\varepsilon_0$

Table 2 shows that the hoop stress range and axial stress range in the free expansion case ($\varepsilon_{zz}=\varepsilon_0$) have the same critical frequency, f=0.3 Hz. For fixed axial strain ($\varepsilon_{zz}=0$), the critical frequency for axial stress range is f_{cr}=0.1Hz, lower than for free expansion, and gives a higher value of axial stress range. From this reason, in the case of fully circumferential crack, we use only fixed axial case (most conservative) for crack growth analysis.

In reference [32] the lifetimes of the same configuration under thermomechanical loading with different frequencies are compared to determine a critical interval of loading

frequency for crack growth. The frequencies around 0.1 Hz were found to be critical for crack growth of circumferential crack, consistent with the present analysis.

The corresponding stress profiles, obtained by using Equations (28, 29, 30) with the critical frequency values already mentioned, are displayed in Figures 6, 7, and 8 for instants of time during the cycles with extreme values of stresses (in compression and tension) at inner surface. The same figures include both the smoothed polynomial fits and original analytical function predictions for the associated thermal stresses.

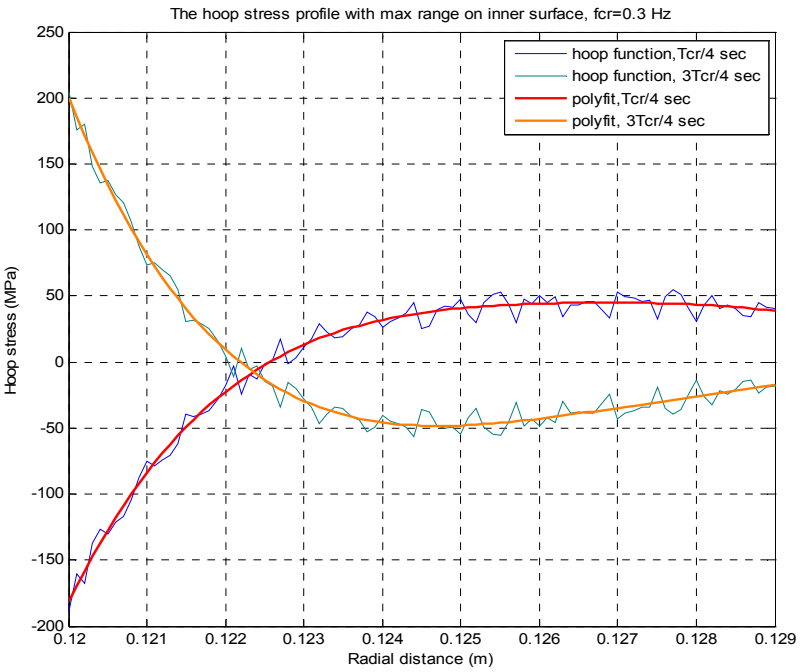

Figure 6. The hoop stress distribution through wall-thickness with maximum range on inner surface (f_{cr}=0.3 Hz).

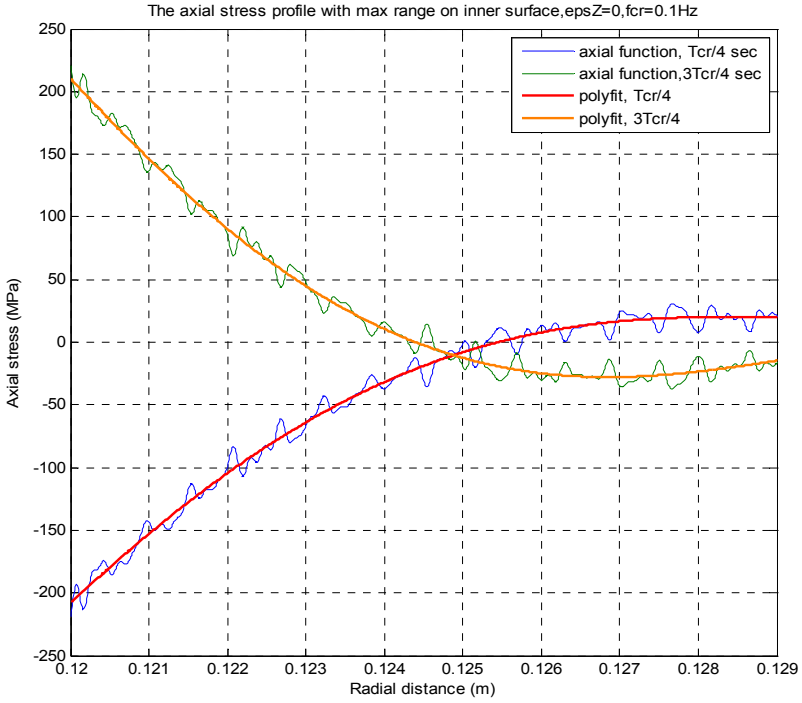

Figure 7. The axial stress distribution through wall-thickness with maximum range on inner surface (f_{cr}=0.1 Hz, ε_z=0)

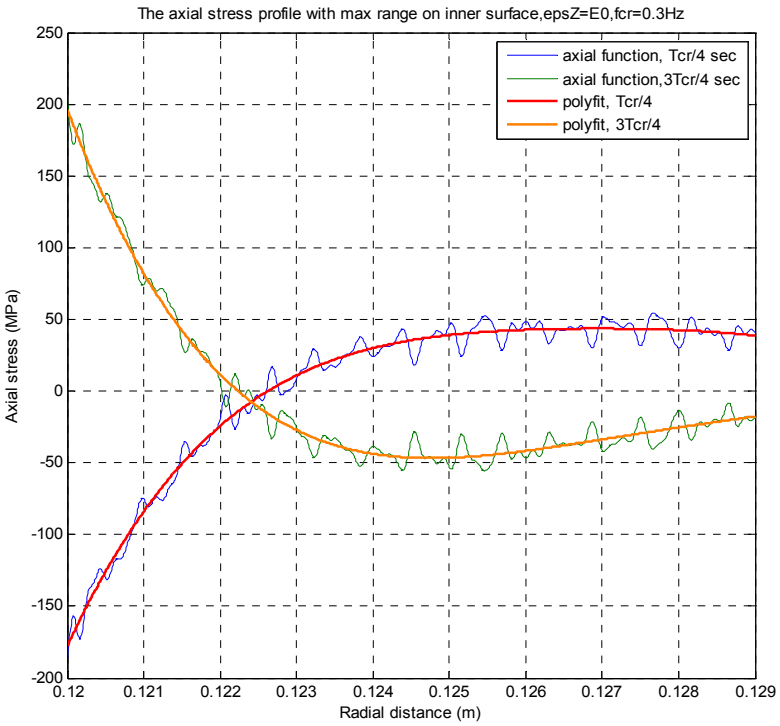

Figure 8. The axial stress distribution through wall-thickness with maximum range on inner surface (f_{cr}=0.3 Hz, ε_z=ε_0).

An interesting task, from the fatigue crack initiation point of view, was to perform the same analysis for the effective stress intensities. Fatigue crack initiation in

components subjected to multiaxial stress states is assessed by the various codes and standards [1, 33, 34]] by using of these specific stress-related parameters. The definition of this parameter is typically based on a maximum shear stress yield criterion (Tresca) or a maximum distortion energy yield criterion (von Mises). This latter is the most used, and therefore the following additional scalar stress parameters are evaluated at the critical frequencies:

- effective stress intensity (Von Mises equivalent stress):

$$\sigma_{VM} = \sqrt{\frac{(\sigma_r - \sigma_\theta)^2 + (\sigma_z - \sigma_\theta)^2 + (\sigma_r - \sigma_z)^2}{2}} \tag{47}$$

- effective equivalent stress range intensity (for application with a maximum distortion energy yield criterion in fatigue crack initiation):

$$\Delta S_{range} = \sqrt{\frac{(\Delta\sigma_r - \Delta\sigma_\theta)^2 + (\Delta\sigma_z - \Delta\sigma_\theta)^2 + (\Delta\sigma_r - \Delta\sigma_z)^2}{2}} \tag{48}$$

The values obtained are given in Table 3. Figures 9 and 10 show the frequency dependence of effective stress intensity (σ_{VM}) and effective equivalent stress range intensity (ΔS_{VM}) in both conditions: axial fixed (ε_z=0) and axial free (ε_z=ε_0).

Table 3. Critical frequencies for effective stress range intensities in pipe inner surface under sinusoidal thermal loading

Stress	Critical frequency (Hz)	Stress (MPa)	Axial boundary conditions
Maximum effective stress intensity (σ_{VM})	0.21 0.38	201 186	ε_z=0 ε_z=ε_0
Maximum effective equivalent stress range intensity (ΔS_{VM})	0.25 0.30	410 386	ε_z=0 ε_z=ε_0

For the mixing tee zone of the Civaux 1 structure (were the crack leak was produced), reference [1] reported that the equivalent stress distributions (in Von Mises sense) at the inner surface reached a maximum value of 358 MPa. This is consistent with the

prediction here of ΔS_{VM} = 386 MPa, obtained at the critical frequency of sinusoidal thermal loading and for the fixed axial boundary condition (Table 3).

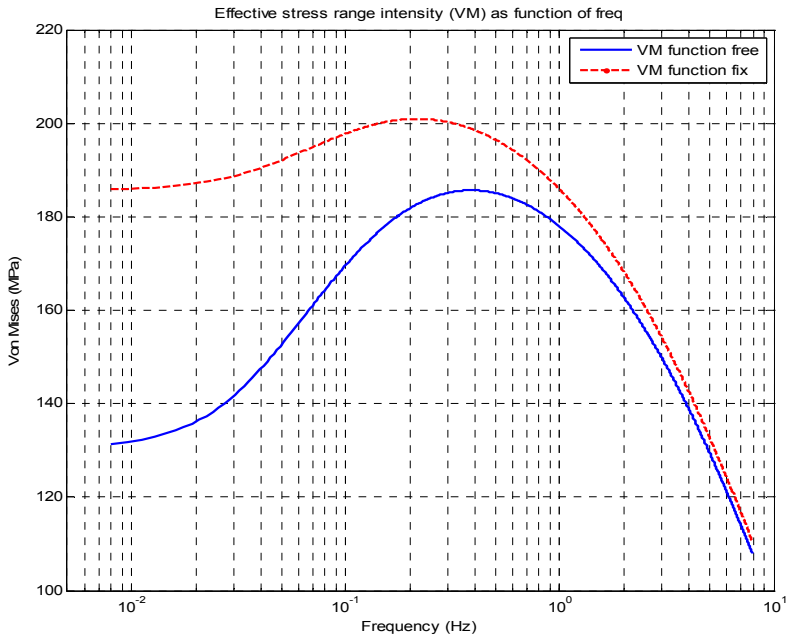

Figure 9. Dependence of maximum equivalent stress intensity (σ_{VM}) on thermal loading frequencies (Civaux case)

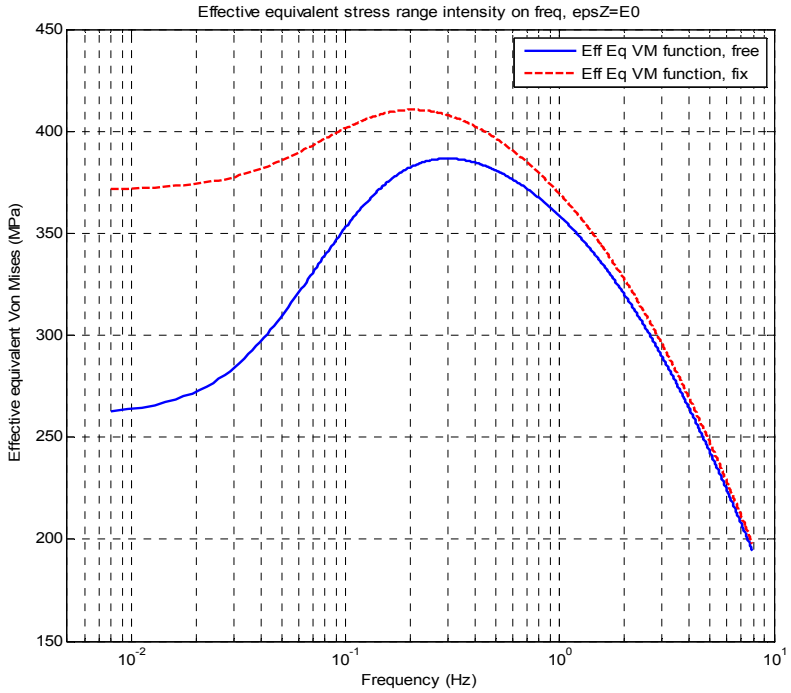

Figure 10. Dependence of maximum effective equivalent stress range intensity (ΔS_{VM}) on thermal loading frequencies (Civaux case)

In summary, the critical frequencies (in sense of maximum range stress at inner surface) for sinusoidal thermal loading are $f \in$[0.1, 0.3] Hz for the axial and hoop elastic

thermal stress components and $f \in [0.21, 0.38]$ Hz for equivalent stress intensities. These results are in agreement with those reported in literature [5, 7, 10, 11], which consider the interval $f \in [0.1, 1.0]$ Hz to be most damaging for thermal fatigue in high cycle domain. In ref [10, 11] the value f=0.5 Hz was considered as most critical frequency. In the next steps of analyses we use the stress profiles (maximum values) for hoop stress and axial stress (ε_z=0 case) at the critical frequencies given in Table 2.

4.3.2 Stress intensity factor solution for long axial crack under hoop thermal stress

To check the analytical prediction of the through-thickness hoop stress profile during thermal loading a comparison of FEA and analytical results was performed for f_{cr}=0.3 Hz (Figure 11). From an ABAQUS output file, which comprises stress values for discrete values of time during a period of thermal loading, a specific instant of time was chosen to that as close as possible in the FE output file to that at which the inner surface stress was maximum.

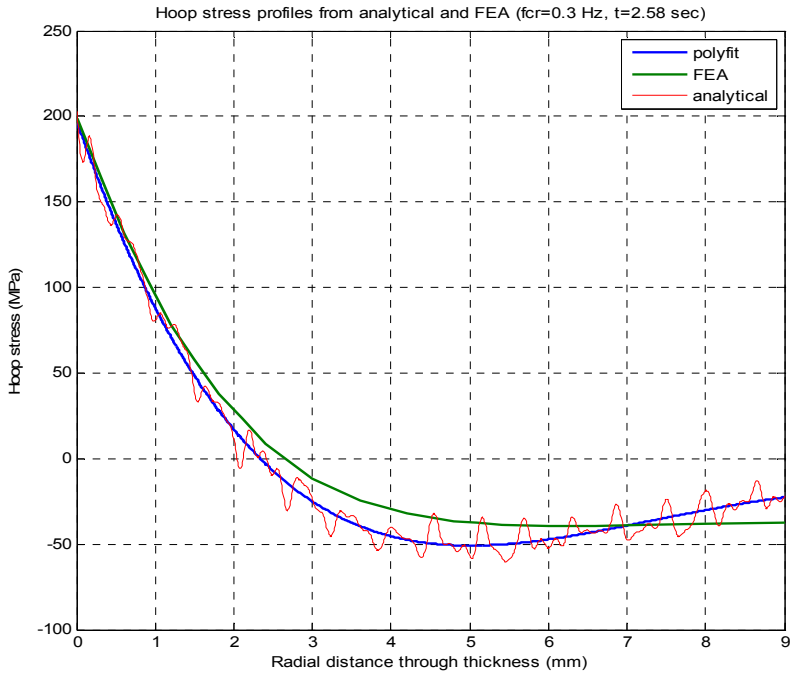

Figure 11. Comparison between hoop stress profiles from FEA and analytical methods for f_{cr}=0.3 Hz

There is a small difference between analytical prediction (either the function itself or the corresponding polynomial fit) and FEA results in the middle region of wall-thickness,

where the values of hoop stress are already in negative domain. It is worth mentioning that the stress gradients through the thickness are similar. Note: the instant of time used here does not correspond to that at which the maximum stress occurs on the inner surface.

In the case of evaluation of the Mode I stress intensity factor in a pipe, K_{laxial}, for an infinite longitudinal surface crack under thermal hoop stress, the procedure from reference [31] was followed, which uses the following relation:

$$K_{Iaxial}(\frac{a}{l}) = \left[G_0\sigma_0 + G_1\sigma_1\left(\frac{a}{l}\right) + G_2\sigma_2\left(\frac{a}{l}\right)^2 + G_3\sigma_3\left(\frac{a}{l}\right)^3 + G_4\sigma_4\left(\frac{a}{l}\right)^4 \right]\sqrt{\frac{\pi a}{Q}} \qquad (49)$$

where G_0, G_1, G_2, G_3, G_4 are influence coefficients, and $Q=1$ for this configuration. In our application for the pipe geometry of the Civaux 1 case, the inner radius/wall-thickness ratio is $\frac{r_i}{l} \approx 13$. The corresponding values of the influence coefficients of stress distribution do not be found directly from Table C9 of API 579 procedure [31]. Therefore, it is necessary to perform an interpolation to infer the influence coefficients G_0, G_1, G_2, G_3, G_4, for mentioned pipe geometry. Table 4 displays the published values in the range of interest [31].

Table 4 The influence coefficients of stress distribution for a longitudinal infinite length surface crack in a cylindrical shell from Table C9 -API 579

r_i/l	a/l	G_0	G_1	G_2	G_3	G_4
5	0.0 0.2 0.4 0.6 0.8	1.12 1.307452 1.8332 2.734052 3.940906	0.682 0.753466 0.954938 1.28757 1.739955	0.5245 0.564296 0.676408 0.857474 1.10621	0.4404 0.466913 0.539874 0.656596 0.81823	0.379075 0.398757 0.454785 0.54072 0.661258
10	0.0 0.2 0.4 0.6 0.8	1.12 1.332691 1.957764 3.223438 5.543784	0.682 0.763153 1.002123 1.466106 2.300604	0.5245 0.569758 0.702473 0.953655 1.398958	0.4404 0.470495 0.556857 0.718048 1.000682	0.379075 0.401459 0.467621 0.585672 0.789201
20	0.0 0.2 0.4 0.6 0.8	1.12 1.345621 2.028188 3.573882 7.388754	0.682 0.768292 1.028989 1.594673 2.946567	0.5245 0.57256 0.717256 1.023108 1.736182	0.4404 0.472331 0.566433 0.762465 1.211533	0.379075 0.402984 0.475028 0.618437 0.936978

r_i – inner radius; l- wall-thickness

The results of cubic spline interpolation (MATLAB function) for the influence coefficients of stress distribution in case of ratio $\frac{r_i}{l} \approx 13$ are shown in Table 5.

Table 5. Results of cubic spline interpolations for influence coefficients of hoop stress distribution for the case of an infinite axial crack on inner pipe surface case

r_i/l	a/l	G_0	G_1	G_2	G_3	G_4
13	0.0	1.12	0.682	0.5245	0.4404	0.379075
13	0.2	1.3418	0.7667	0.5717	0.4718	0.4025
13	0.4	2.0039	1.0196	0.7121	0.5631	0.4724
13	0.6	3.4165	1.5367	0.9917	0.7424	0.6035
13	0.8	6.2878	2.5609	1.5349	1.0855	0.8487

As can be seen in Table 5, each influence coefficient needs a new interpolation as function of the $\frac{a}{l}$ ratio, in order to consider the dependence of the stress intensity factor K_{laxial} on crack depth *a*. The following relationships give the required dependence:

$$G_0\left(\frac{a}{l}\right) = 10.6083 \cdot \left(\frac{a}{l}\right)^3 - 1.9273 \cdot \left(\frac{a}{l}\right)^2 + 1.2123 \cdot \left(\frac{a}{l}\right) + 1.1143 \quad (50)$$

$$G_1\left(\frac{a}{l}\right) = 3.5302 \cdot \left(\frac{a}{l}\right)^3 - 0.4091 \cdot \left(\frac{a}{l}\right)^2 + 0.4166 \cdot \left(\frac{a}{l}\right) + 0.6799 \quad (51)$$

$$G_2\left(\frac{a}{l}\right) = 1.775 \cdot \left(\frac{a}{l}\right)^3 - 0.11 \cdot \left(\frac{a}{l}\right)^2 + 0.215 \cdot \left(\frac{a}{l}\right) + 0.5234 \quad (52)$$

$$G_3\left(\frac{a}{l}\right) = 1.0823 \cdot \left(\frac{a}{l}\right)^3 - 0.0284 \cdot \left(\frac{a}{l}\right)^2 + 0.1364 \cdot \left(\frac{a}{l}\right) + 0.4397 \quad (53)$$

$$G_4\left(\frac{a}{l}\right) = 0.7044 \cdot \left(\frac{a}{l}\right)^3 + 0.056 \cdot \left(\frac{a}{l}\right)^2 + 0.0914 \cdot \left(\frac{a}{l}\right) + 0.3785 \quad (54)$$

A check was performed comparing the stress intensity factor calculated by means of the methodology described above with that from finite element analysis results. In Appendix 4 a comparison between analytical predictions of K_{laxial} for long axial crack under hoop

stress due to internal pressure and FEA results are shown. The solutions for K_{laxial} are in a good agreement until the crack depth reaches the 80% from wall-thickness.

For each instant of time during a period of thermal loading, we also need the coefficients of the hoop stress polynomial fit to derive K_{laxial} for long axial crack under hoop thermal stress at frequency f_{cr}=0.3 Hz. The required steps are complete described in full in Appendix 5 for the instant of time corresponding to maximum hoop stress range on inner surface and critical frequency f_{cr}=0.3 Hz. The steps described in Appendix 5 are used to generate through-wall stress profiles for several instants of time during a thermal loading cycle. These are curve-fitted by a fourth order polynomial distribution for each instant of time. The frequency f_{cr}=0.3 Hz was considered. The general form of the fourth order polynomial distribution is as given by Equation (42).

Figures 12 and 13 show the hoop stress profiles at several instants of time from T/2 to T, and also from T to 3T/2, respectively (where T is the period of the thermal loading cycle). The stress distributions available as 4th order polynomials were transformed to be consistent with the wall thickness coordinate in normalized form.

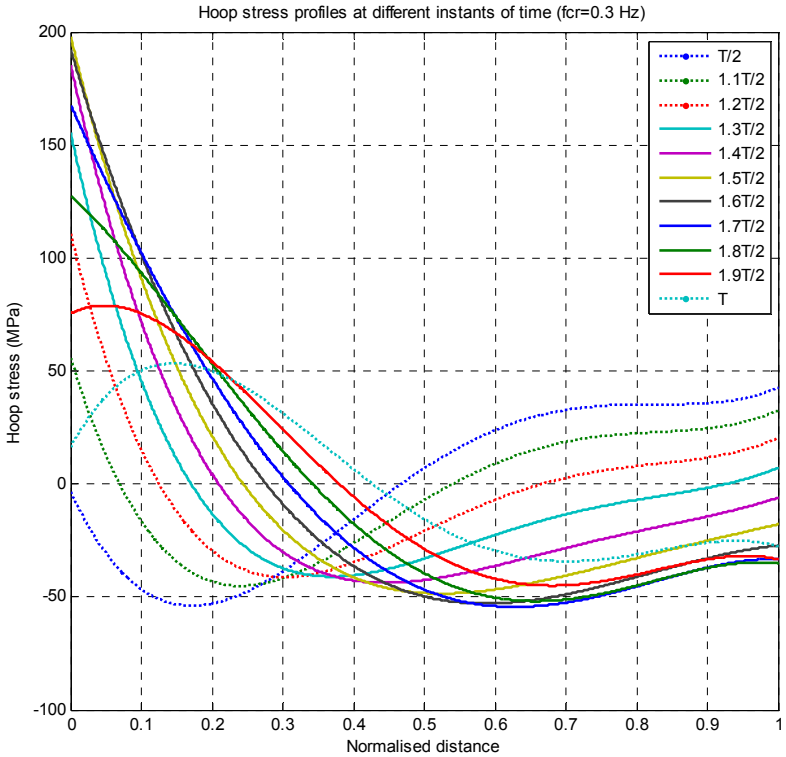

Figure 12. Through-wall hoop stress profiles (f_{cr}=0.3 Hz), at various instants of time as function of normalized x/l distance (between T/2 and T)

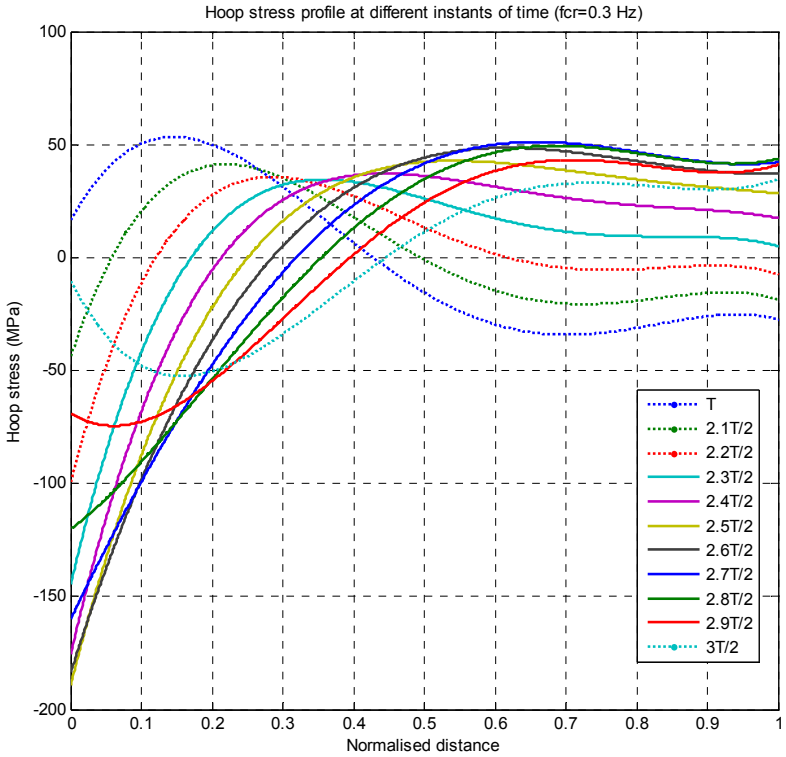

Figure 13. Through-wall hoop stress profiles (f_{cr}=0.3 Hz), at various instants of time as function of normalized x/l distance (between T and 3T/2)

This process the polynomial fits to be extracted and Table 6 provides the resulting values of the coefficients derived for hoop stress profiles shown in Figures 12 and 13.

Table 6. Coefficients of polynomial fitting for hoop stress profiles at various instants of time during a period of sinusoidal thermal loading

	σ_0	σ_1	σ_2	σ_3	σ_4
T/2	-3.3768	-673.9602	2765.1309	-3459.4409	1414.2546
1.1T/2	55.951	-1020.8664	3337.5666	-3851.2798	1511.26
1.2T/2	110.6402	-1276.251	3595.9905	-3867.3872	1457.431
1.3T/2	155.2782	-1413.8301	3511.7821	-3503.7995	1257.6864
1.4T/2	185.44.4	-1419.1325	3090.7992	-2794.6168	931.4656
1.5T/2	198.1231	-1290.841	2372.519	-1808.3494	510.7206
1.6T/2	192.0368	-1040.8689	1425.9824	-641.0138	36.7302
1.7T/2	167.733	-693.156	342.9057	593.392	-443.9745
1.8T/2	127.549	-281.2985	-771.3884	1774.1315	-884.1841
1.9T/2	75.38	154.7597	-1808.3465	2785.6047	-1240.6439

T	16.2967	572.6517	-2666.8514	3528.7031	-1478.2951
2.1T/2	-43.9507	931.7458	-3263.1647	3930.5379	-1573.7106
2.2T/2	-99.4957	1197.1314	-3539.1379	3951.5945	-1517.3915
2.3T/2	-144.9299	1343.0424	-3467.9279	3589.6133	-1314.6981
2.4T/2	-175.8325	1355.3841	-3056.6366	2879.8207	-985.326
2.5T/2	-189.2035	1233.1173	-2345.6261	1891.4874	-561.379
2.6T/2	-183.7569	988.3622	-1404.5746	721.1522	-84.2265
2.7T/2	-160.0472	645.2151	-325.6618	-516.8249	399.5462
2.8T/2	-120.4153	237.3911	785.4507	-1701.4548	842.6981
2.9T/2	-68.7588	-195.0747	1819.9588	-2716.9619	1201.9568
3T/2	-10.1514	-609.7445	2676.5646	-3464.1157	1442.255

By using the influence coefficients (Equations 50 to 54) and the coefficients of the polynomial fit to the hoop stress profiles (Table 6) we are able to derive K_{Iaxial} for long axial crack under hoop thermal stress at frequency f_{cr}=0.3 Hz (see Equation 49). Figures 14 and 15 show the dependence of K_{Iaxial} on crack depth through thickness at different instants of time during a period of thermal loading.

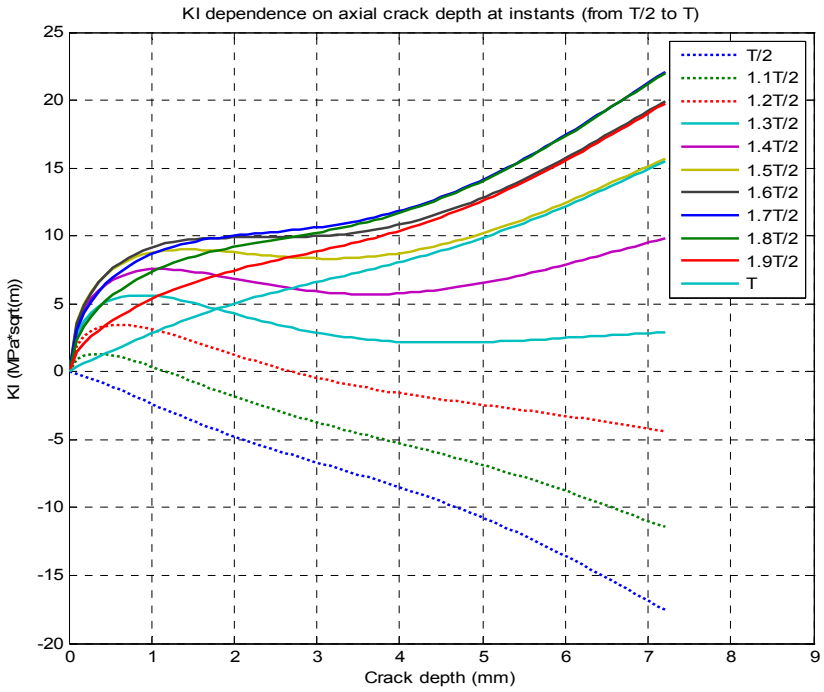

Figure 14. Dependence of K_{Iaxial} for long axial crack under hoop stress at different instants of time between T/2 and T (f_{cr}=0.3 Hz)

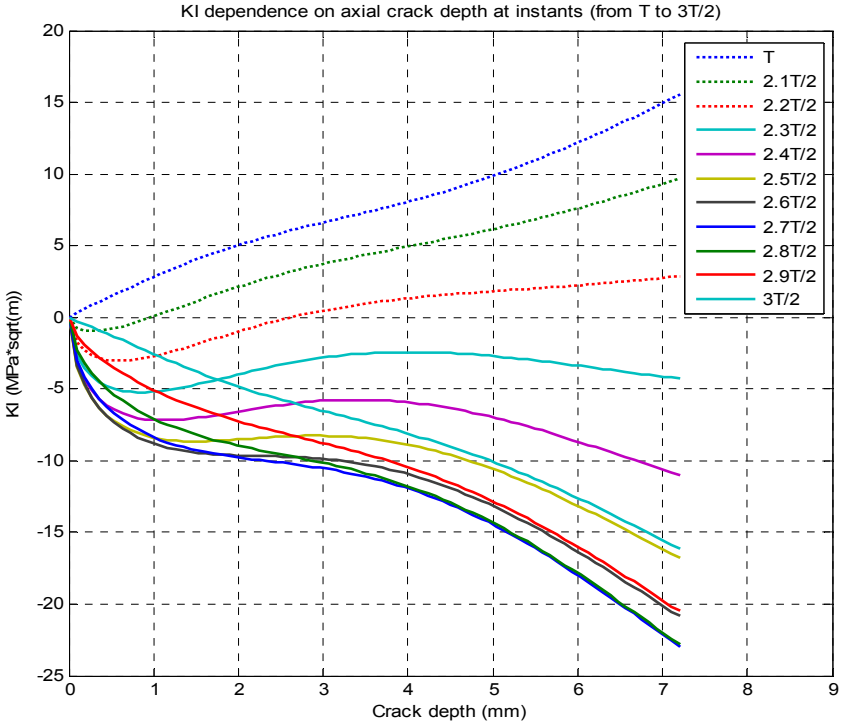

Figure 15. Dependence of K_{Iaxial} for long axial crack under hoop stress at different instants of time between T and 3T/2 (f_{cr}=0.3 Hz)

Figure 16 compares the maximum stress intensity values predicted in Figures 14 and 15 with those obtained by finite element method (ABAQUS analysis) as a function of crack depth starting from the inner surface of the pipe wall.

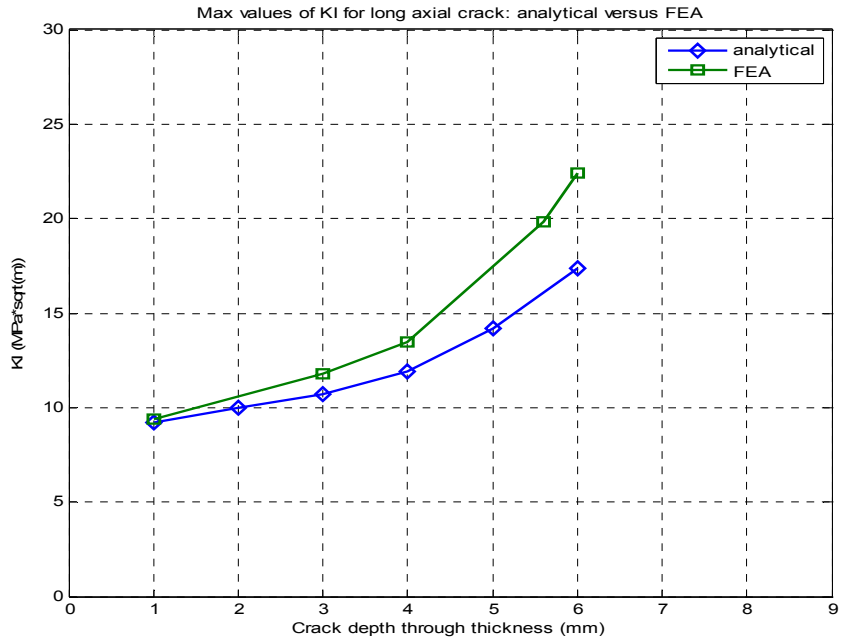

Figure 16. Comparison of $K_{Iaxial}^{\max}$ for long axial crack: FEA versus analytical (f_{cr}=0.3Hz)

To apply the generalized Paris law for crack growth propagation it is convenient to express the dependence on crack depth as polynomial function for both assessment:

$$K_{Iaxial}^{\max}(analyt) = 33333333.3333 \cdot a^3 - 40476.1905 \cdot 10^4 \cdot a^2 + 440.4762 \cdot a + 8.8429 \qquad (55)$$

$$K_{Iaxial}^{\max}(FEA) = 181756397.2617 \cdot a^3 - 1356696.4107 \cdot a^2 + 4306.2857 \cdot a + 6.2582 \qquad (56)$$

where $K_{Iaxial}^{\max}$ is in MPa√m and crack depth *a* is in m. These equations will be used with the Paris law integration to compute crack growth propagation time.

4.3.3 Stress intensity factor solution for fully circumferential crack under axial thermal stress

Appendix 6 describes all the steps for deriving the stress intensity factor for a fully circumferential crack for an instant of time which corresponds to the maximum axial stress on inner pipe surface (ε_0=0, f_{cr}=0.1 Hz). Figure 17 shows a comparison between FEA and analytical predictions of the stress distribution.

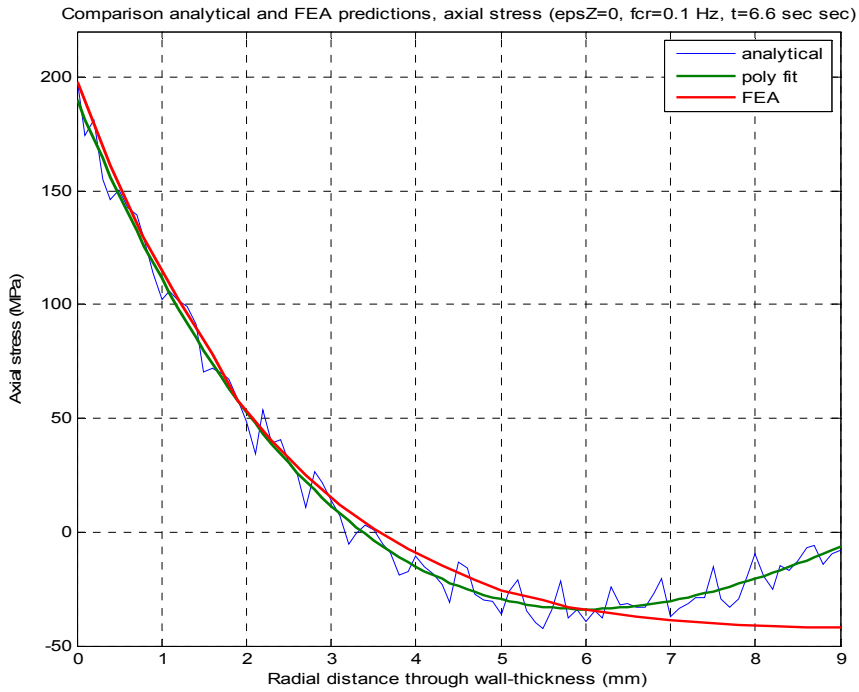

Figure 17. Comparison between axial stress profiles from FEA and analytical for f_{cr}=0.1 Hz (ε_0=0)

The Mode I stress intensity factor for fully circumferential surface crack, K_{Icirc}, is:

$$K_{Icirc}(\frac{a}{l}) = \left[G'_0 \sigma'_0 + G'_1 \sigma'_1 \left(\frac{a}{l}\right) + G'_2 \sigma'_2 \left(\frac{a}{l}\right)^2 + G'_3 \sigma'_3 \left(\frac{a}{l}\right)^3 + G'_4 \sigma'_4 \left(\frac{a}{l}\right)^4 \right] \sqrt{\frac{\pi a}{Q}} \qquad (57)$$

where G'_0, G'_1, G'_2, G'_3, G'_4 are influence coefficients of axial stress distribution, and $Q=1$ also for this configuration,. As already mentioned, for the pipe geometry of Civaux 1 case, the ratio of inner radius to thickness is $\frac{r_i}{l} \approx 13$. By performing a cubic spline interpolation, the influence coefficients G'_0, G'_1, G'_2, G'_3, G'_4 were computed. Table 7 shows these in the range of interest, for fully circumferential crack in the pipe.

Table 7 Influence coefficients of axial stress distribution for a fully circumferential surface crack in a cylindrical shell from Table C10 - API 579

r_i/l	a/l	G'_0	G'_1	G'_2	G'_3	G'_4
5	0.0	1.12	0.682	0.5245	0.4404	0.379075
	0.2	1.210829	0.718943	0.546312	0.454558	0.390464
	0.4	1.437161	0.807345	0.596196	0.487609	0.415918
	0.6	1.764266	0.928708	0.656426	0.519455	0.447584
	0.8	2.272892	1.156841	0.801593	0.627635	0.528369
10	0.0	1.12	0.682	0.5245	0.4404	0.379075
	0.2	1.254559	0.735816	0.555784	0.46081	0.395216
	0.4	1.578769	0.860586	0.625575	0.506771	0.43019
	0.6	2.054427	1.033913	0.712856	0.555383	0.47372
	0.8	2.691796	1.302652	0.877596	0.675063	0.561238
20	0.0	1.12	0.682	0.5245	0.4404	0.379075
	0.2	1.286308	0.748129	0.562711	0.465393	0.398716
	0.4	1.700591	0.906527	0.650941	0.523329	0.442578
	0.6	2.354964	1.143036	0.771413	0.592683	0.500911
	0.8	3.202288	1.480478	0.970278	0.732879	0.601399

r_i – inner radius; l- wall-thickness

The results of cubic spline interpolation at $\frac{r_i}{l} \approx 13$ for influence coefficients of axial stress distribution are shown in Table 8.

Table 8. Results of spline interpolations for influence coefficients: the radial-circumferential 360^0 crack on inner pipe surface

r_i/l	a/l	G'_0	G'_1	G'_2	G'_3	G'_4
13	0.0	1.12	0.682	0.5245	0.4404	0.379075
13	0.2	1.2719	0.7425	0.5595	0.4633	0.3971
13	0.4	1.6379	0.8828	0.6379	0.5148	0.4362
13	0.6	2.1838	1.0808	0.7380	0.5714	0.4854
13	0.8	2.8908	1.3719	0.9137	0.6976	0.5769

A 3rd order fit for each of influence coefficient using the data from Table 8, gives the following :

$$G'_0\left(\frac{a}{l}\right) = -0.5521.\left(\frac{a}{l}\right)^3 + 2.9663.\left(\frac{a}{l}\right)^2 + 0.1938.\left(\frac{a}{l}\right) + 1.1198 \quad (58)$$

$$G'_1\left(\frac{a}{l}\right) = 0.1385.\left(\frac{a}{l}\right)^3 + 0.7604.\left(\frac{a}{l}\right)^2 + 0.1654.\left(\frac{a}{l}\right) + 0.6812 \quad (59)$$

$$G'_2\left(\frac{a}{l}\right) = 0.3354.\left(\frac{a}{l}\right)^3 + 0.1388.\left(\frac{a}{l}\right)^2 + 0.1608.\left(\frac{a}{l}\right) + 0.5234 \quad (60)$$

$$G'_3\left(\frac{a}{l}\right) = 0.4271.\left(\frac{a}{l}\right)^3 - 0.1345.\left(\frac{a}{l}\right)^2 + 0.1557.\left(\frac{a}{l}\right) + 0.4391 \quad (61)$$

$$G'_4\left(\frac{a}{l}\right) = 0.2211.\left(\frac{a}{l}\right)^3 + 0.0151.\left(\frac{a}{l}\right)^2 + 0.0937.\left(\frac{a}{l}\right) + 0.3785 \quad (62)$$

For the stress profiles, the general form of fourth order polynomial distribution, given by Equation (42), was used at the critical frequency f_{cr}=0.1 Hz. The same instants of time were used as in previous section and the results derived from Figures 18 and 19 are shown in Table 9.

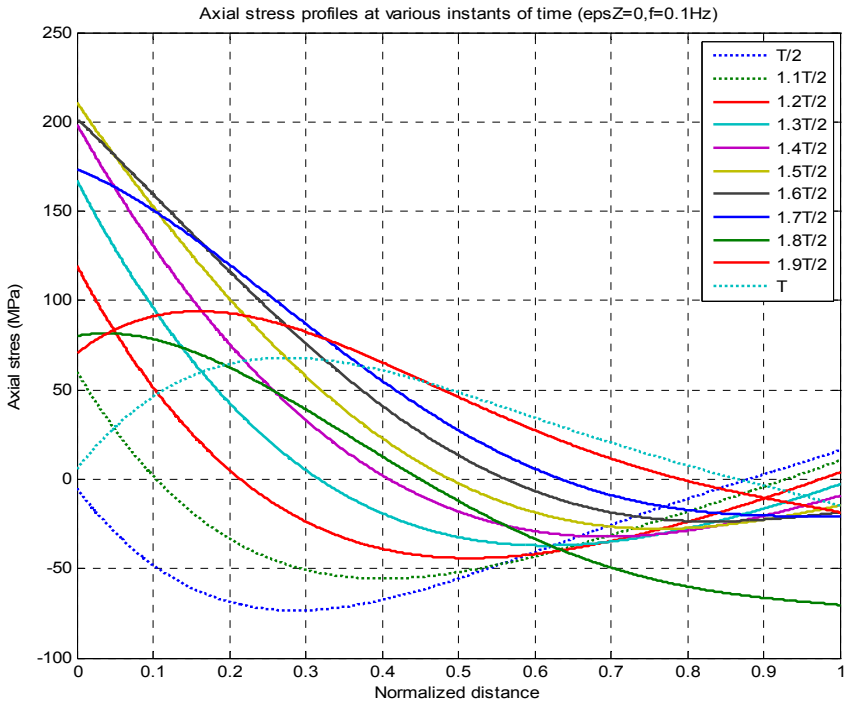

Figure 18. Through-wall axial stress (ε_z=0 and f_{cr}=0.1 Hz) at various instants of time as function of normalized *x/l* distance (between T/2 and T)

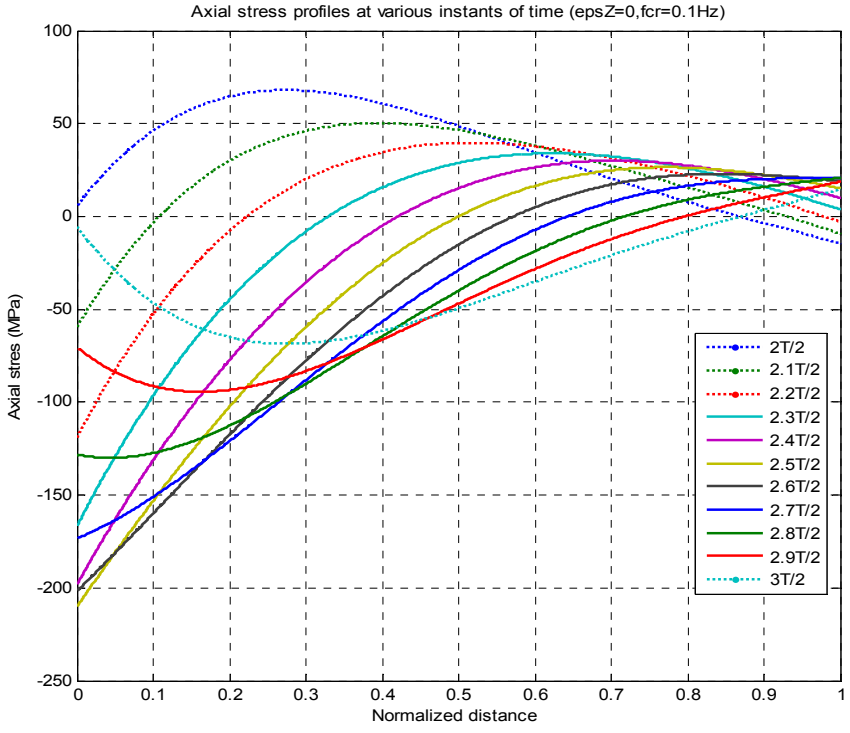

Figure 19. Through-wall axial stress (ε_z=0 and f_{cr}=0.1 Hz) at various instants of time as function of normalized *x/l* distance (between T and 3T/2)

Table 9. Coefficients of polynomial fitting for axial stress profiles at various instants of time during a period of sinusoidal loading (f_{cr}=0.1 Hz, ε_0=0)

	σ'_0	σ'_1	σ'_2	σ'_3	σ'_4
T/2	-4.9075	-565.5558	1485.14	-1328.7272	430.2012
1.1T/2	60.2403	-719.9045	1486.5824	-1166.3144	349.8424
1.2T/2	119.5714	-806.5893	1342.8453	-884.2742	232.3383
1.3T/2	167.2621	-816.5557	1067.912	-511.2958	89.7714
1.4T/2	198.6312	-748.3767	688.6368	-84.7623	-63.438
1.5T/2	210.5979	-608.3667	242.1039	352.8728	-211.9203
1.6T/2	201.9824	-409.9442	-228.0085	758.2085	-340.8435
1.7T/2	173.6216	-172.3033	-675.707	1091.1177	-437.3498
1.8T/2	80.2023	75.5051	-1065.7869	2343.3267	-503.5368
1.9T/2	70.4103	326.7004	-1335.1218	1418.2548	-498.7183
T	5.6554	539.48	-1482.3175	1379.9425	-457.3
2.1T/2	-59.6426	699.0805	-1484.3752	1207.2831	-371.5043
2.2T/2	-119.0937	789.9536	-1341.1011	917.0308	-249.6519
2.3T/2	-166.8804	803.2636	-1066.5261	537.4081	-103.6086
2.4T/2	-198.3262	737.7552	-687.5325	105.6903	52.3794
2.5T/2	-210.3541	599.8789	-241.2228	-336.147	203.0826
2.6T/2	-201.7876	-403.1612	228.7121	-744.8415	333.7808
2.7T/2	-173.4659	166.8827	676.2691	-1080.4352	431.7055
2.8T/2	-128.162	-85.8087	1057.6361	-1310.1162	487.2914
2.9T/2	-70.3109	-330.1622	1335.4807	-1411.4322	495.1136
3T/2	-5.5759	-542.2466	1482.6043	-1374.4902	454.4193

In order to determine stress intensity factor, K_{Icirc} , the influence coefficients (Equations 58 to 62) and coefficients of polynomial fitting (Table 9) were substituted into Equation 57. Figure 20 and 21 show the K_{Icirc} dependence on crack depth at different instants of time, as noted in Table 9.

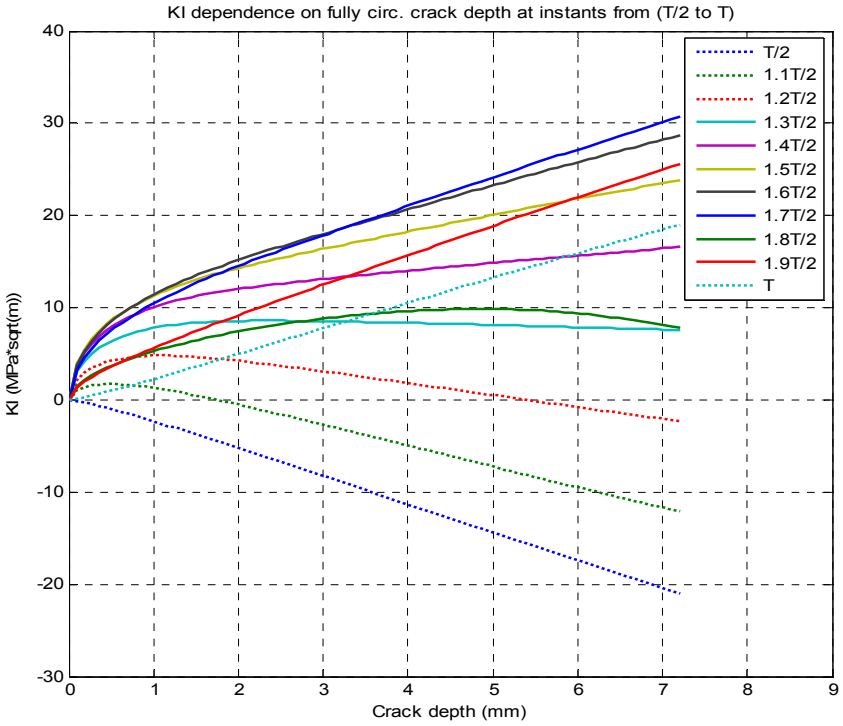

Figure 20 Dependence of K_{Icirc} on crack depth for fully circumferential crack under axial stress at different instants of time between T/2 and T (f_{cr}=0.1 Hz, ε_0=0)

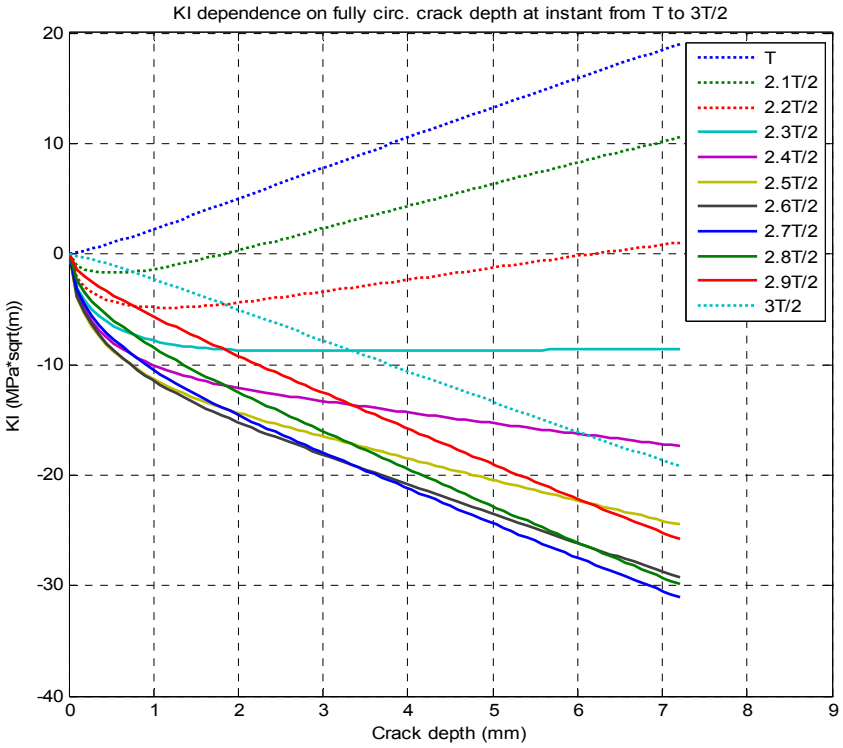

Figure 21 Dependence of K_{Icirc} on crack depth for fully circumferential crack under axial stress at different instants of time between T and 3T/2 (f_{cr}=0.1 Hz, ε_0=0)

The maximum values for K_{Icirc} from analytical predictions (Figure 20), during a period of thermal loading were compared with FEA results. Figure 22 shows the good agreement obtained.

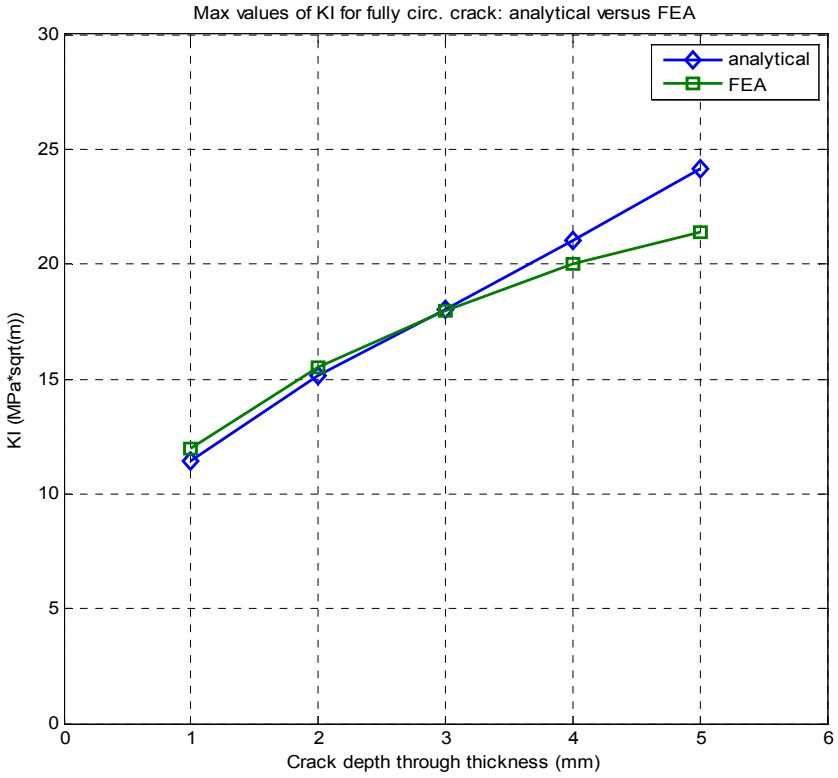

Figure 22. Comparison for $K_{Icirc}^{\max}$ for fully circumferential crack: FEA and analytical (f_{cr}=0.1 Hz, ε_0=0)

It is convenient to express dependency of stress intensity factor $K_{Icirc}^{\max}$ on crack depth from Figure 22 as polynomial functions of crack depth:

$$K_{Icirc}^{\max}(analyt) = 79166666.6667 \cdot a^3 - 805357.1429 \cdot a^2 + 5515.4762 \cdot a + 6.68 \quad (63)$$

$$K_{Icirc}^{\max}(FEA) = -16666666.6667 \cdot a^3 - 235714.2857 \cdot a^2 + 4180.9524 \cdot a + 8.08 \quad (64)$$

where $K_{Icirc}^{\max}$ is in MPa√m and crack depth *a* is in m. These equations will be used in the integration of the Paris law equation to compute the crack growth propagation time.

4.3.4 Fatigue life assessment for crack growth

The fatigue crack growth life assessment in our approach is based on the hypothesis that during thermal cycling a crack grows when at crack tip experiences the maximum value of K_I . A crack growth threshold, ΔK_{th}=5.06 MPa$\sqrt{m}$ was assumed. To obtain the rate of crack growth in case of long axial crack we apply a generalized Paris law, as is used in reference [1]:

$$\frac{da}{dN} = C.\left(\Delta K_{eff}\right)^n . \tag{65}$$

The constant are referred as : C= 7.5 x 10^{-13} (m/cycle) and n= 4 [1].

Based on the hypothesis already mentioned, ΔK_{eff} is expressed as function of the maximum stress intensity factor range for the relevant crack geometry.
The effective stress intensity factor range is also dependent on the stress ratio and in the case with (*R<0)* ΔK_{eff} the following approach is considered [1]

$$\Delta K_{eff} = q(R).\Delta K_I . \tag{66}$$

and $$q(R) = \frac{1-0.5.R}{1-R} . \tag{67}$$

The analytical model predicts an approximately symmetrical response of thermal hoop stress about the zero state. Hence by setting

$$K_{Iaxial}^{\min} = -K_{Iaxial}^{\max} . \tag{68}$$

the range of stress intensity factor becomes

$$\Delta K_{Iaxial} = 2 \cdot K_{Iaxial}^{\max} . \tag{69}$$

In the meantime: *R=-1* and *q=3/4* (70)

With above results the effective stress intensity factor is

$$\Delta K_{eff} = q\Delta K_{Iaxial} = \frac{3}{2} K_{Iaxial}^{\max} \quad . \tag{71}$$

To compute the crack growth propagation time, Equation (65) is integrated between the limits a_i (initial crack depth) and a_f (final crack depth). The same values used were as in reference [1]: a_i*=1 mm* and a_f*=7.2 mm*, that means in term of crack/thickness ratio a_i/l*=0.1 and* a_f/l*=0.8*. The number of cycles (*N*) required to advance a crack between a_i and a_f is given by:

$$N = \int_{ai}^{af} \frac{da}{C(\Delta K_{eff}(a))^n} \tag{72}$$

The corresponding time (T) in hours is given by

$$T(hours) = \frac{N}{3600 \cdot f_{cr}} \tag{73}$$

Table 10 shows the results obtained for a critical frequency f_{cr}=0.3 Hz.The results obtained in reference [1] are also includes .

Table 10 Comparison of crack growth time predictions for long axial crack subjected to thermal hoop stress (f_{cr}=0.3 Hz)

Method	Number of cycles to propagate a crack to 80% of wall thickness	Time (hours) to propagate a crack to 80% of wall thickness
Analytical	88 263	82
FEA	59 294	55
Chapuliot, et al. [1]	372 720	517

The results from the analytical and FEA approaches are in quite good agreement. They are conservative in comparison with those obtained in more advanced approaches referred [1]. We have to note that CEA results [1] were obtained in the following conditions: the stresses were obtained from an analysis of the full pipe elbow geometry and the K_I factors were derived from a plate model.

The same methodology as above was performed for a fully circumferential crack, using Equations (63, 64) and Equation (72). Table 11 compares the results of the present work and the Chapuliot et al. [1].

Table 11 Comparison of crack growth time predictions for fully circumferential crack subjected to thermal axial stress (f_{cr}=0.1 Hz, ε_0=0)

Method	Number of cycles to propagate a crack to 80% of wall thickness	Time (hours) to propagate a crack to 80% of wall thickness
Analytical	16 161	45
FEA	17 762	49
Chapuliot et al. [1]	21 388	59

It is considered that our simple approach to derive the thermal fatigue crack growth life gives conservative results because it used only the most critical frequencies from the loading spectra, i.e. these producing the maximum stress ranges.

5. Summary and Conclusions

An analytical method for fatigue crack growth assessment in a pipe subject to sinusoidal thermal loading has been successfully developed and implemented in a MATLAB software environment.

Its application is explained via analysis of the Civaux 1 case. Additionally, finite element analyses were used to check the thermal stress profiles and the stress intensity factors derived from the analytical model.

The critical sine wave frequency is calculated for both the axial and hoop stress components from the value that produces the maximum tensile stress component at the inner surface (0.1 and 0.3 Hz, respectively). Using 4^{th} order polynomial fits of these through-wall stress distributions the corresponding stress intensity factors for a long axial crack and fully circumferential crack were calculated for a range of crack depths using the *K* solutions given in API 579 procedure. The maximum range of stress intensity factors during a period of thermal loading, expressed as a function of crack depth is substituted in a Paris law to obtain thermal fatigue crack growth life.

Agreement with results from independent assessment of Civaux case was demonstrated, although it must be noted the predictions from the present work are lower bound to these. This conservatism is explained by the use of only the critical frequencies to represent the entire loading spectrum.

A beneficial aspect of this type of analytical solution in case of thermal stripping modeling is the fact that they can be easily manipulated in check the influence of various parameters (critical frequency, thermal stress component, crack geometry etc.) in a systematic way. They provide a useful option for initial assessments of real problems minimizing the need more time consuming finite element analyses.

References

[1] S. Chapuliot et al. *Hydro-thermal-mechanical analysis of thermal fatigue in a mixing tee*, Nuclear Engineering and Design 235 (2005) 575-596

[2] O. Ancelet, et al. *Development of a test for the analyses of the harmfulness of 3D thermal fatigue loading in tubes*, International Journal of Fatigue 29 (2007), 549-564

[3] B. Drubay, et al *A 16: guide for defect assessment at elevated temperature*, International Journal of Pressure Vessels and Piping 80 (2003) 499-516

[4] N. Haddar *Thermal fatigue crack networks: an computational study*, International Journal of Solids and Structures 42(2005) 771-788

[5] IAEA-TECDOC-1361, *Assessment and management of ageing of major nuclear power plant components important to safety-primary piping in PWRs*, IAEA, July 2003

[6] Lin-Wen Hu, et al., *Numerical Simulation study of high thermal fatigue caused by thermal stripping, Third International Conference on Fatigue of Reactor Components,* Seville, Spain 3-6 October 2004, NEA/CSNI/R(2004)21

[7] Naoto Kasahara et al. *Structural response function approach for evaluation of thermal stripping phenomena*, Nuclear Engineering and Design 212 (2002) 281-292

[8] B.A. Boley, J. Weiner, *Theory of Thermal Stresses*, John Wiley & Sons, 1960

[9] M. Dahlberg et al. *Development of a European Procedure for Assessment of High Cycle Thermal Fatigue in Light Water Reactors: Final Report of the NESC-Thermal Fatigue Project*, NESC Network Report NESC-06-04, published as European Commission EUR 22763 EN June 2007

[10] D. Buckthorpe, O. Gelineau, M.W.J. Lewis, A. Ponter, *Final report on CEC study on thermal stripping benchmark –thermo mechanical and fracture calculation*, Project C5077/TR/001, NNC Limited 1988

[11] H.-Y.Lee, J.-B. Kim, B. Yoo *Tee-Junction of LMFR secondary circuit involving thermal, thermomechanical and fracture mechanics assessment on a stripping phenomenon*, IAEA-TECDOC-1318, “Validation of fast reactor thermomechanical and thermohydraulic codes”, Final report of a coordinated research project 1996-1999 (1999)

[12] V. Radu, E. Paffumi, N. Taylor, *New analytical stress formulae for arbitrary time dependent thermal loads in pipes,* European Commission Report EUR 22802 DG JRC, June 2007, Petten, NL

[13] N. Noda, R.B. Hetnarski, Y. Tanigawa, *Thermal Stresses*, 2nd Ed., Taylor & Francis, 2003

[14] S.P. Timoshenko, J.N. Goodier, *Theory of Elasticity*, McGraw-Hill, New York, (1987)

[15] I.N. Sneddon, *The Use of Integral Transforms*, McGraw-Hill, New York, (1993)

[16] M. Garg, A.Rao, S.L. Kalla, *On a generalized finite Hankel transform*, Applied Mathematics and Computation (2007), doi:10.1016/j.amc.2007.01.076

[17] A.R. Shahani, S.M. Nabavi, *Analytical solution of the quasi-static thermoelasticity problem in a pressurized thick-walled cylinder subjected to transient thermal loading*, Applied Mathematical Modelling (2006), doi:10.1016/j.apm.2006.06.008

[18] Bahram Farahmand *Fatigue and Fracture Mechanics of High Risk parts: Application of LEFM& FMDM Theory*, Chapman & Hall, 1997

[19] X. J. Zheng, et al. *Weight functions and stress intensity factors for internal surface semi-elliptical crack in thick-walled cylinder*, Engineering Fracture Mechanics vol. 58, No. 3, pp 207-221 (1997)

[20] A.A. Moftakhar, G. Glinka *Calculation of stress intensity factors by efficient integration of weight functions*, Engineering Fracture Mechanics vol. 43, No. 5, pp 7497-756 (1992)

[21] A. Kiciak, G. Glinka, D.J. Burns *Calculation of Stress Intensity Factors and Crack opening Displacements for Cracks Subjected to Complex Stress Fields*, ASME Journal Pressure Vessels Technology 2003; 124:261-6

[22] I.S. Jones *"Impulse response model of thermal striping for hollow cylindrical geometries*, Theoretical and applied fracture mechanics 43 (2005) 77-88

[23] I.S. Jones, G. Rothwell *Reference stress intensity factors with application to weight functions for internal circumferential cracks in cylinders*, Engineering Fracture Mechanics 68 (2001) 435-454

[24] H.J. Petroski, J.D. Achenbach *Computation of the weight function from a stress intensity factor*, Engineering Fracture Mechanics, 1978, vol.18, 257-266

[25] A.R.Shahani, S.E. Habibi *Stress intensity factors in a hollow cylinder containing a circumferential semi-elliptical crack subjected to combined loading*, International Journal of Fatigue 29 (2007) 128-140

[26] A.R. Shahani, S.M. Nabavi *Closed form stress intensity factors for a semi-elliptical crack in a thick-walled cylinder under thermal stress*, International Journal of Fatigue 28 (2006) 926-933

[27] A.R. Shahani, S.M. Nabavi *Transient thermal stress intensity factors for an internal longitudinal semi-eliptical crack in a thick-walled cylinder*, Engineering Fracture Mechanics (2007), doi:10.1016/j.engfracmech.2006.11.018

[28] H. Grebner, U. Strathmeier *Stress intensity factors for longitudinal semi-elliptical surface cracks in a pipe under thermal loading*, Engineering Fracture Mechanics, vol. 21, No.2, pp.383-389, 1985

[29] R. Oliveira, X.R. Wu *Stress intensity factors for axial cracks in hollow cylinders subjected to thermal shock*, Engineering Fracture Mechanics, vol. 27, No.2, pp.185-197, 1987

[30] Toshiyuki Meshii, Katsuhiko Watanabe *Stress intensity factors evaluation of a circumferential crack in a finite length thin-walled cylinder for arbitrarily distributed stress on crack surface by weight function method*, Nuclear Engineering and Design 2006 (2001) 13-20

[31] API 579 Fitness-for-Service-API *Recommended Practice 579, First Edition, January 2000*, American Petroleum Institute

[32] Mohammad Seydi, Said Taheri, Francois Hild *Numerical modeling of crack propagation and shielding effects in a striping network*, Nuclear Engineering and Design 236 (2006) 954-964

[33] Brian B. Kerezsi, John W.H. Price, *Using the ASME and BSI codes to predict crack growth due to repeated thermal shock*, International Journal of Pressure Vessels and Piping 79 (2002) 361-371

[34] O.K. Chopra, W.J. Shack *Effect of LWR Coolant Environments on the fatigue Life of reactor Materials, Draft report for Comment*, NUREG/CR-6909, ANL 06/08, July 2006, U.S. Nuclear Regulatory Commission , Office of Nuclear Regulatory Research, Washington, DC 20555-0001

[35] S.R.Gosselin, F.A. Simonen, P.G. Heasler, S.R. Doctor *Fatigue Crack Flaw Tolerance in Nuclear Power Plant Piping – A Basis for Improvements to ASME Code Section XI Appendix L*, NUREG/CR-6934, PNNL-16192, May 2007

Appendix 1: Thermal stress components for a pipe subject to sinusoidal thermal loading

The integrals I_1 and I_2 for the sinusoidal case are:

$$I_1(r,\omega,t)=\int_{r_i}^{r}\theta(r,t)\cdot r\cdot dr=k\cdot\pi\cdot\sum_{n=1}^{\infty}\frac{s_n^2\cdot J_0^2(s_n\cdot r_o)}{J_0^2(s_n\cdot r_o)-J_0^2(s_n\cdot r_i)}\times$$
$$\times\left[\frac{1}{s_n}\left\{Y_o(s_n\cdot r_i)\cdot\left[r\cdot J_1(s_n\cdot r)-r_i\cdot J_1(s_n\cdot r_i)\right]-J_o(s_n\cdot r_i)\cdot\left[r\cdot Y_1(s_n\cdot r)-r_i\cdot Y_1(s_n\cdot r_i)\right]\right\}\right]\times$$
$$\times\left[\theta_0\cdot\frac{\omega\cdot e^{-k\cdot s_n^2\cdot t}+(k\cdot s_n^2)\cdot\sin(\omega\cdot t)-\omega\cdot\cos(\omega\cdot t)}{(k\cdot s_n^2)^2+\omega^2}\right] \tag{A1.1}$$

$$I_2(\omega,t)=\int_{r_i}^{r_o}\theta(r,t)\cdot r\cdot dr=k\cdot\pi\cdot\sum_{n=1}^{\infty}\frac{s_n^2\cdot J_0^2(s_n\cdot r_o)}{J_0^2(s_n\cdot r_o)-J_0^2(s_n\cdot r_i)}\times$$
$$\times\left[\frac{1}{s_n}\left\{Y_o(s_n\cdot r_i)\cdot\left[r_o\cdot J_1(s_n\cdot r_o)-r_i\cdot J_1(s_n\cdot r_i)\right]-J_o(s_n\cdot r_i)\cdot\left[r_o\cdot Y_1(s_n\cdot r_o)-r_i\cdot Y_1(s_n\cdot r_i)\right]\right\}\right]\times$$
$$\times\left[\theta_0\cdot\frac{\omega\cdot e^{-k\cdot s_n^2\cdot t}+(k\cdot s_n^2)\cdot\sin(\omega\cdot t)-\omega\cdot\cos(\omega\cdot t)}{(k\cdot s_n^2)^2+\omega^2}\right] \tag{A1.2}$$

where s_n are the positive roots of the transcendental equation

$$Y_o(s_n\cdot r_i)\cdot J_o(s_n\cdot r_o)-J_o(s_n\cdot r_i)\cdot Y_o(s_n\cdot r_o)=0 \quad . \tag{A1.3}$$

The thermal stress components for a hollow circular cylinder subject to sinusoidal thermal loading are:

Hoop thermal stress

$$\sigma_\theta(r,\omega,t)=\frac{\alpha\cdot E}{1-\nu}\times\left\{\left(\frac{1}{r^2}\right)k\cdot\pi\cdot\sum_{n=1}^{\infty}\frac{s_n^2\cdot J_0^2(s_n\cdot r_o)}{J_0^2(s_n\cdot r_o)-J_0^2(s_n\cdot r_i)}\times\right.$$
$$\times\left[\frac{1}{s_n}\left\{Y_o(s_n\cdot r_i)\cdot\left[r\cdot J_1(s_n\cdot r)-r_i\cdot J_1(s_n\cdot r_i)\right]-J_o(s_n\cdot r_i)\cdot\left[r\cdot Y_1(s_n\cdot r)-r_i\cdot Y_1(s_n\cdot r_i)\right]\right\}\right]\times$$
$$\times\left[\theta_0\cdot\frac{\omega\cdot e^{-k\cdot s_n^2\cdot t}+(k\cdot s_n^2)\cdot\sin(\omega\cdot t)-\omega\cdot\cos(\omega\cdot t)}{(k\cdot s_n^2)^2+\omega^2}\right]+\frac{r^2+r_i^2}{r^2(r_o^2-r_i^2)}\times$$
$$\times k\cdot\pi\cdot\sum_{n=1}^{\infty}\frac{s_n^2\cdot J_0^2(s_n\cdot r_o)}{J_0^2(s_n\cdot r_o)-J_0^2(s_n\cdot r_i)}\times$$
$$\times\left[\frac{1}{s_n}\left\{Y_o(s_n\cdot r_i)\cdot\left[r_o\cdot J_1(s_n\cdot r_o)-r_i\cdot J_1(s_n\cdot r_i)\right]-J_o(s_n\cdot r_i)\cdot\left[r_o\cdot Y_1(s_n\cdot r_o)-r_i\cdot Y_1(s_n\cdot r_i)\right]\right\}\right]\times$$
$$\times\left[\theta_0\cdot\frac{\omega\cdot e^{-k\cdot s_n^2\cdot t}+(k\cdot s_n^2)\cdot\sin(\omega\cdot t)-\omega\cdot\cos(\omega\cdot t)}{(k\cdot s_n^2)^2+\omega^2}\right]-$$
$$-k\cdot\pi\cdot\sum_{n=1}^{\infty}\frac{s_n^2\cdot J_0^2(s_n\cdot r_o)}{J_0^2(s_n\cdot r_o)-J_0^2(s_n\cdot r_i)}\left[Y_o(s_n\cdot r_i)\cdot J_o(s_n\cdot r)-J_o(s_n\cdot r_i)\cdot Y_o(s_n\cdot r)\right]\times$$
$$\left.\times\left[\theta_0\cdot\frac{\omega\cdot e^{-k\cdot s_n^2\cdot t}+(k\cdot s_n^2)\cdot\sin(\omega\cdot t)-\omega\cdot\cos(\omega\cdot t)}{(k\cdot s_n^2)^2+\omega^2}\right]\right\}$$

(A1.4)

Axial thermal stress

for $\varepsilon_z=0$ (fixed end)

$$\sigma_z(r,\omega,t)=\frac{\alpha\cdot E}{1-\nu}\left\{\frac{2\nu}{r_i^2-r_o^2}\times k\cdot\pi\cdot\sum_{n=1}^{\infty}\frac{s_n^2\cdot J_0^2(s_n\cdot r_o)}{J_0^2(s_n\cdot r_o)-J_0^2(s_n\cdot r_i)}\times\right.$$
$$\times\left[\frac{1}{s_n}\left\{Y_o(s_n\cdot r_i)\cdot\left[r_o\cdot J_1(s_n\cdot r_o)-r_i\cdot J_1(s_n\cdot r_i)\right]-J_o(s_n\cdot r_i)\cdot\left[r_o\cdot Y_1(s_n\cdot r_o)-r_i\cdot Y_1(s_n\cdot r_i)\right]\right\}\right]\cdot$$
$$\cdot\left[\theta_0\cdot\frac{\omega\cdot e^{-k\cdot s_n^2\cdot t}+(k\cdot s_n^2)\cdot\sin(\omega\cdot t)-\omega\cdot\cos(\omega\cdot t)}{(k\cdot s_n^2)^2+\omega^2}\right]-$$
$$-k\cdot\pi\cdot\sum_{n=1}^{\infty}\frac{s_n^2\cdot J_0^2(s_n\cdot r_o)}{J_0^2(s_n\cdot r_o)-J_0^2(s_n\cdot r_i)}\left[Y_o(s_n\cdot r_i)\cdot J_o(s_n\cdot r)-J_o(s_n\cdot r_i)\cdot Y_o(s_n\cdot r)\right]\times$$
$$\left.\times\left[\theta_0\cdot\frac{\omega\cdot e^{-k\cdot s_n^2\cdot t}+(k\cdot s_n^2)\cdot\sin(\omega\cdot t)-\omega\cdot\cos(\omega\cdot t)}{(k\cdot s_n^2)^2+\omega^2}\right]\right\}$$

(A1.5)

for $\varepsilon_z=\varepsilon_0$ (free end)

$$\sigma_z(r,\omega,t)=\frac{\alpha\cdot E}{1-\nu}\left\{\frac{2}{r_i^{\,2}-r_o^{\,2}}\times k\cdot\pi\cdot\sum_{n=1}^{\infty}\frac{s_n^2\cdot J_0^2(s_n\cdot r_o)}{J_0^2(s_n\cdot r_o)-J_0^2(s_n\cdot r_i)}\times\right.$$

$$\times\left[\frac{1}{s_n}\left\{Y_o(s_n\cdot r_i)\cdot\left[r_o\cdot J_1(s_n\cdot r_o)-r_i\cdot J_1(s_n\cdot r_i)\right]-J_o(s_n\cdot r_i)\cdot\left[r_o\cdot Y_1(s_n\cdot r_o)-r_i\cdot Y_1(s_n\cdot r_i)\right]\right\}\right]\cdot$$

$$\cdot\left[\theta_0\cdot\frac{\omega\cdot e^{-k\cdot s_n^2\cdot t}+(k\cdot s_n^2)\cdot\sin(\omega\cdot t)-\omega\cdot\cos(\omega\cdot t)}{(k\cdot s_n^2)^2+\omega^2}\right]-$$

$$-k\cdot\pi\cdot\sum_{n=1}^{\infty}\frac{s_n^2\cdot J_0^2(s_n\cdot r_o)}{J_0^2(s_n\cdot r_o)-J_0^2(s_n\cdot r_i)}\left[Y_o(s_n\cdot r_i)\cdot J_o(s_n\cdot r)-J_o(s_n\cdot r_i)\cdot Y_o(s_n\cdot r)\right]\times$$

$$\left.\times\left[\theta_0\cdot\frac{\omega\cdot e^{-k\cdot s_n^2\cdot t}+(k\cdot s_n^2)\cdot\sin(\omega\cdot t)-\omega\cdot\cos(\omega\cdot t)}{(k\cdot s_n^2)^2+\omega^2}\right]\right\}$$

(A1.6)

Appendix 2: The first hundred roots of the transcendental equation (Civaux pipe geometry)

For Civaux 1 case, considering a pipe with the inner and outer radii r_i=0.120 m (≅0.1197m) and r_o=0.129 m, the first 100 roots of the transcendental Equation (14) used in the analytical solutions for temperature and stress fields are:

s_n =[337.78; 675.5900; 1.0134e+003; 1.3512e+003; 1.6890e+003;
2.0268e+003; 2.3646e+003; 2.7024e+003; 3.0403e+003; 3.3781e+003;
3.7159e+003; 4.0537e+003; 4.3915e+003; 4.7293e+003; 5.0671e+003;
5.4049e+003; 5.7427e+003; 6.0806e+003; 6.4184e+003; 6.7562e+003;
7.0940e+003; 7.4318e+003; 7.7696e+003; 8.1074e+003; 8.4452e+003;
8.7830e+003; 9.1208e+003; 9.4587e+003; 9.7965e+003; 1.0134e+004;
1.0472e+004; 1.0810e+004; 1.1148e+004; 1.1486e+004; 1.1823e+004;
1.2161e+004; 1.2499e+004; 1.2837e+004; 1.3175e+004; 1.3512e+004;
1.3850e+004; 1.4188e+004; 1.4526e+004; 1.4864e+004; 1.5201e+004;
1.5539e+004; 1.5877e+004; 1.6215e+004; 1.6553e+004; 1.6890e+004;
1.7228e+004; 1.7566e+004; 1.7904e+004; 1.8242e+004; 1.8580e+004;
1.8917e+004; 1.9255e+004; 1.9593e+004; 1.9931e+004; 2.0269e+004;
2.0606e+004; 2.0944e+004; 2.1282e+004; 2.1620e+004; 2.1958e+004;
2.2295e+004; 2.2633e+004; 2.2971e+004; 2.3309e+004; 2.3647e+004;
2.3984e+004; 2.4322e+004; 2.4660e+004; 2.4998e+004; 2.5336e+004;
2.5674e+004; 2.6011e+004; 2.6349e+004; 2.6687e+004; 2.7025e+004;
2.7363e+004; 2.7700e+004; 2.8038e+004; 2.8376e+004; 2.8714e+004;
2.9052e+004; 2.9389e+004; 2.9727e+004; 3.0065e+004; 3.0403e+004;
3.0741e+004; 3.1078e+004; 3.1416e+004; 3.1754e+004; 3.2092e+004;
3.2430e+004; 3.2768e+004; 3.3105e+004; 3.3443e+004; 3.3781e+004];

By using this set of values in the analytical solutions given by Equations (A1.4, A1.5, A1.6) the corresponding sums will have the same number of terms.

Appendix 3: The specific critical frequencies associated with thermal stress components for a pipe due to sinusoidal thermal loading

The analytical formula for hoop stress under sinusoidal thermal loading is used to determine the critical frequencies associated with geometric points (characterized by the *r* variable) through the wall-thickness.

$$\sigma_\theta(r,\omega,t)=\frac{\alpha\cdot E}{1-\nu}\left[\frac{1}{r^2}\cdot I_1(r,\omega,t)+\frac{r^2+r_i^{\,2}}{r^2\cdot(r_o^{\,2}-r_i^{\,2})}\cdot I_2(\omega,t)-\theta(r,\omega,t)\right] \qquad \text{(A3.1)}$$

These critical frequencies are referred to as *specific* critical frequencies corresponding to the maximum hoop stress range at selected points. We can define the following function as the hoop stress range (between two values at π phase each from other) at each point through thickness by means of

$$DH=abs\left[\sigma_\theta\left(r_k,2\cdot\pi\cdot f,\frac{3}{4\cdot f}\right)-\sigma_\theta\left(r_k,2\cdot\pi\cdot f,\frac{1}{4\cdot f}\right)\right] \quad . \qquad \text{(A3.2)}$$

The above function has been studied by keeping r_k constant and varying the frequency *f* between f=0.01 Hz and 10 Hz. The frequency at which the positive maximum of function *DH* occurs gives the specific critical frequency, $f_{cr}\ (r_k)$, at the point r_k through the wall-thickness. Figures A3.1 to A3.7 show the dependence of the function (A3.2) on frequency range at different points through thickness, starting at the inner surface (*r*=0.120m) and continuing up to 6 mm depth (r=0.126 m).

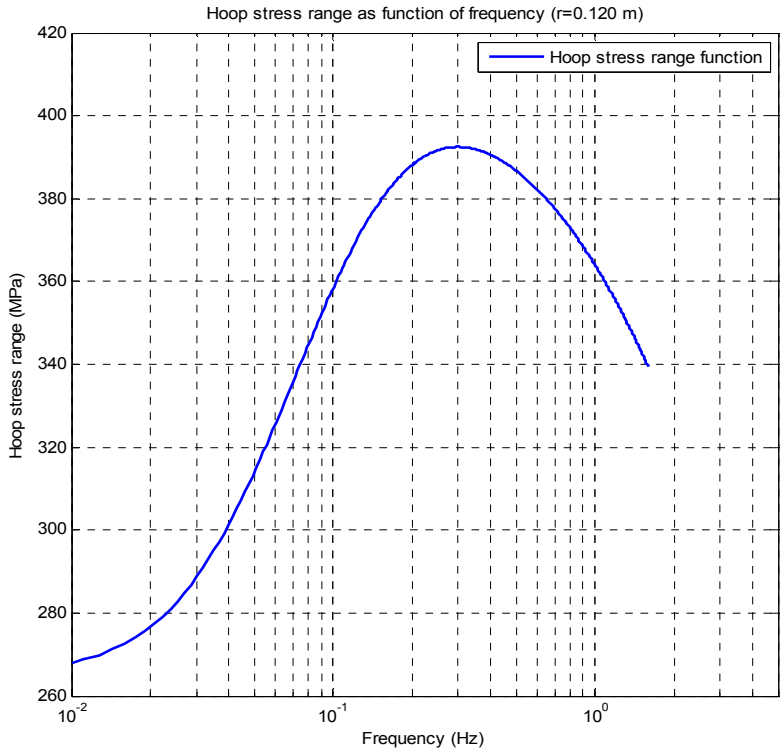

Figure A3.1 Hoop stress range: r=0.120 m, f_{cr}=0.3 Hz

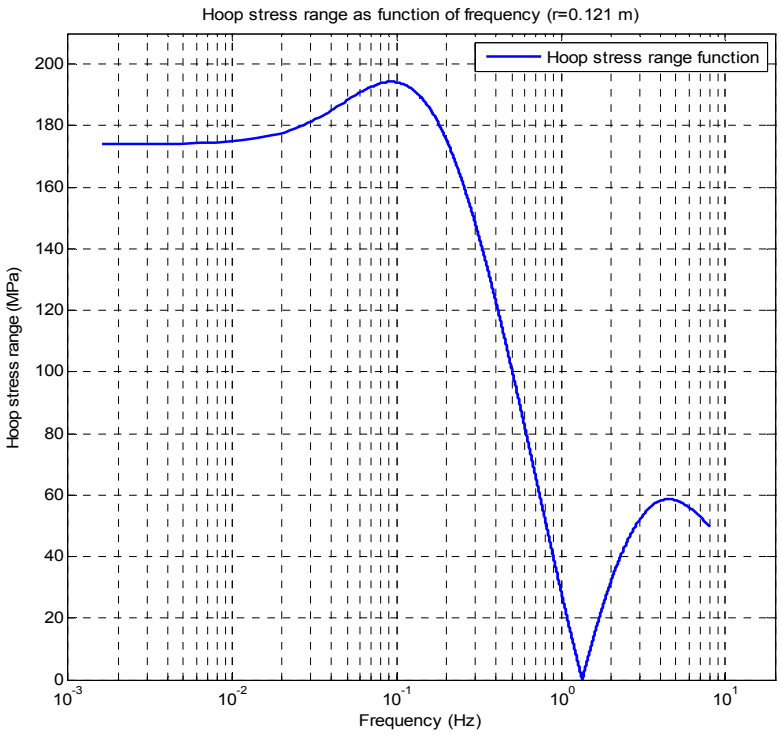

Figure A3.2 Hoop stress range: r=0.121 m, f_{cr}=0.1 Hz, f'_{cr}=4.5 Hz

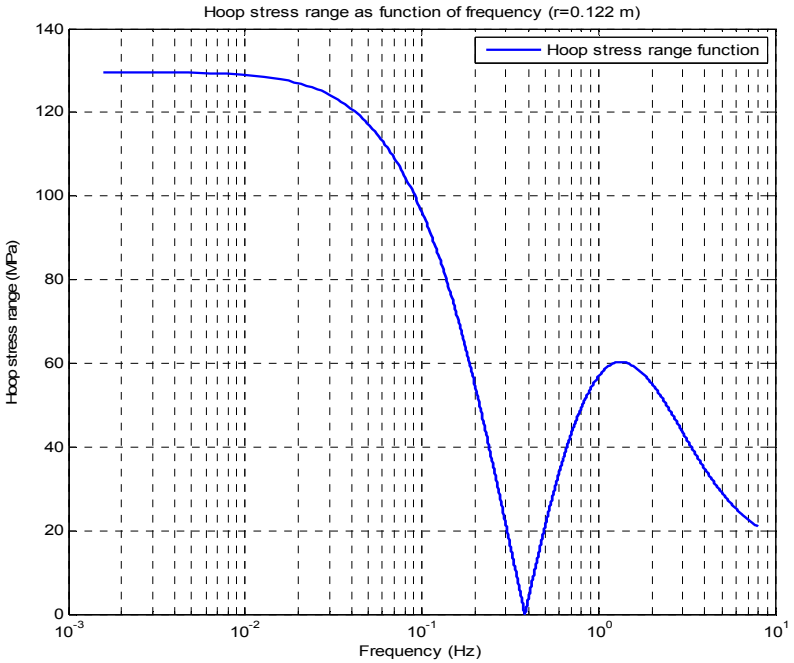

Figure A3.3 Hoop stress range: r=0.122 m, f_{cr}=0.01 Hz, f'_{cr}=1.3 Hz

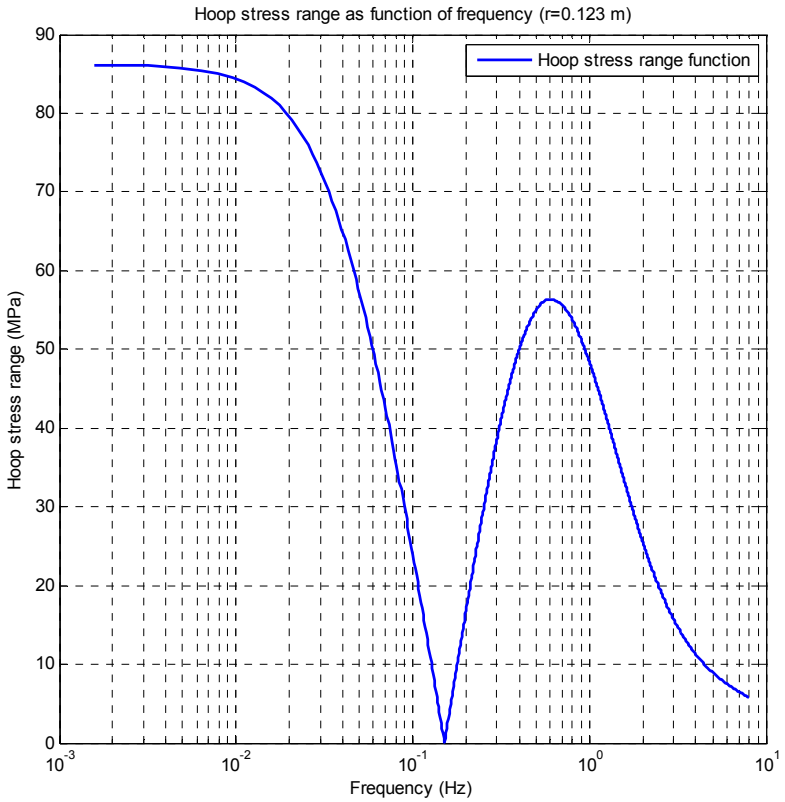

Figure A3.4 Hoop stress range: r=0.123 m, f_{cr}=0.01 Hz, f'_{cr}=0.6 Hz

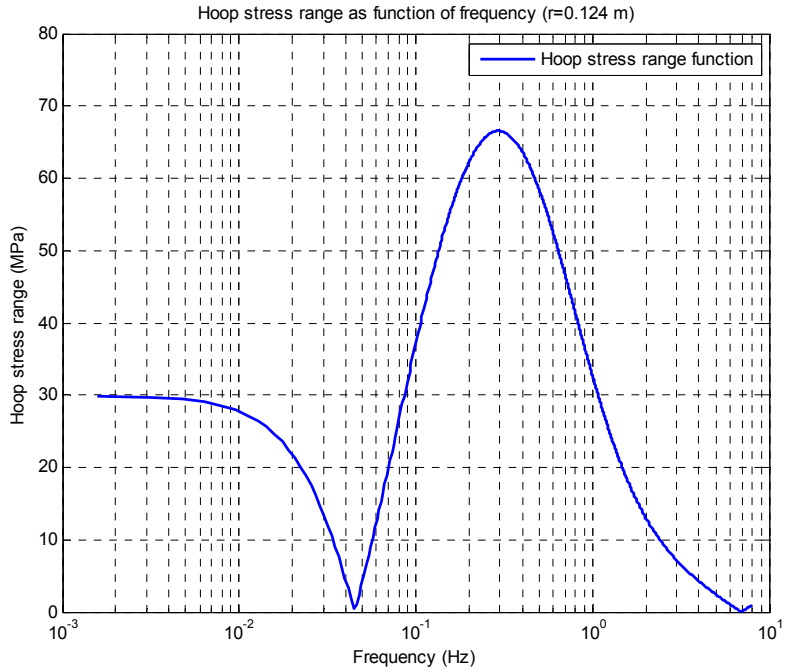

Figure A3.5 Hoop stress range: r=0.124 m, f_{cr}=0.3 Hz

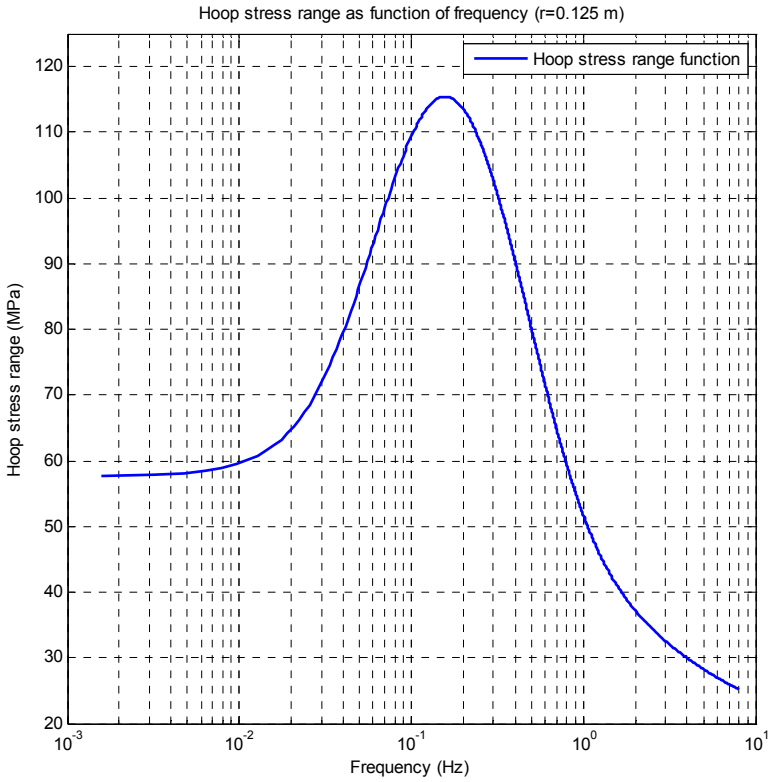

Figure A3.6 Hoop stress range: r=0.125 m, f_{cr}=0.15 Hz

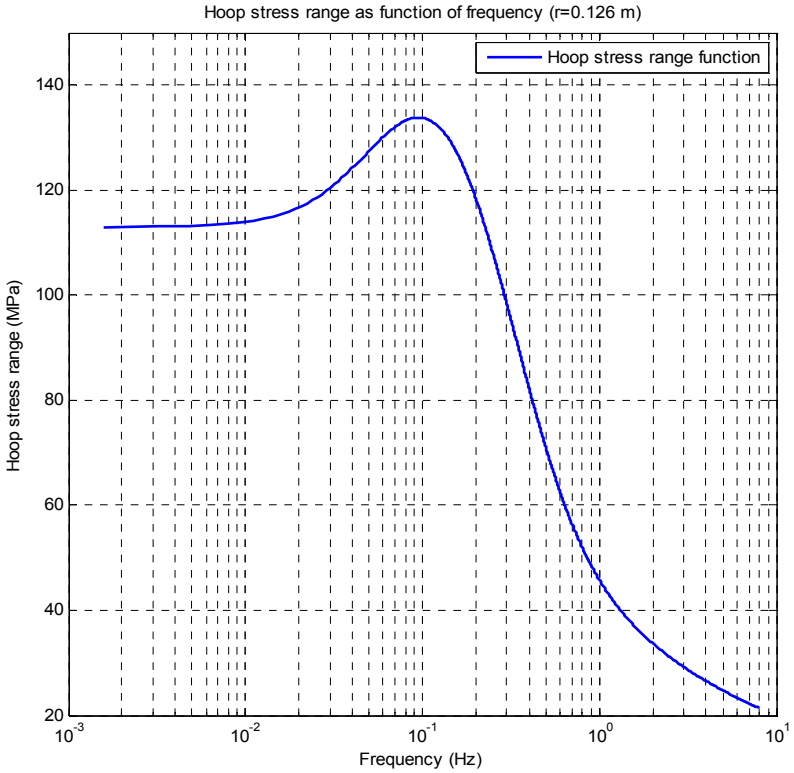

Figure A3.7 Hoop stress range: r=0.126 m, f_{cr}=0.01 Hz

As can be seen from these figures, in several cases there are two specific critical frequencies, for which the maximum values of the DH function are different. For each point through the thickness, we are able to find the maximum stress amplitude during a loading period by applying the analytical function of hoop stress at the specific critical frequency, and after that to derive the maximum stress hoop stress range.

Appendix 4: Benchmarking the stress intensity factor (K_{laxial}) for a long axial crack in a pipe under internal pressure

A simple benchmark was performed to check the prediction of K_{laxial} according to the methodology in section 4.3.2, with a 4th order polynomial distribution of hoop stress, obtained from finite element analysis. A pipe with inner radius r_i=0.120 m and wall thickness 9 mm is assumed to have a long axial crack on its inner surface. The internal pressure is P_i=50 MPa. The radial displacement and hoop stress distributions for the elastic case are given by the analytical solution [14]:

$$u(r) = \frac{(1+\nu)\left[r_i^2 \cdot r_o^2 + r^2(1-2\cdot\nu)\right]P_i}{R \cdot r \cdot \left(r_o^2 - r_i^2\right)} \quad . \tag{A4.1}$$

$$\sigma(\theta) = \frac{E}{(1-2\nu)\cdot(1+\nu)} \cdot \left[(1-\nu)\cdot\frac{u}{r} + \nu \cdot \frac{\partial u}{\partial r}\right] \quad . \tag{A4.2}$$

Figure A4.1 shows the comparison between the analytical profile (Equation A4.2) and FEA results (ABAQUS).

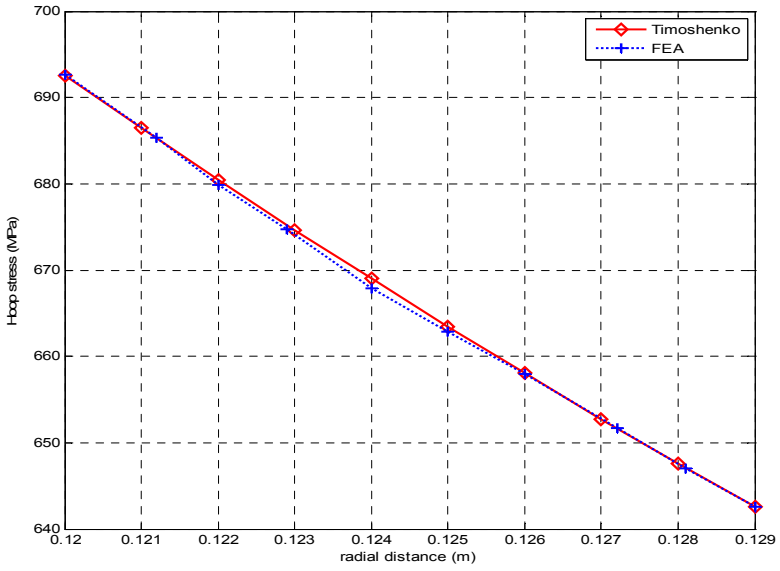

Figure A4.1 Hoop stress through thickness at internal pressure: P=50MPa (Civaux case)

The profile from Figure A4.1 allows us to fit coefficients of a 4th polynomial function and then to use them in Equation 49 (following the methodology already mentioned). The dependence of K_{laxial} on crack depth is shown in Figure A4.2.

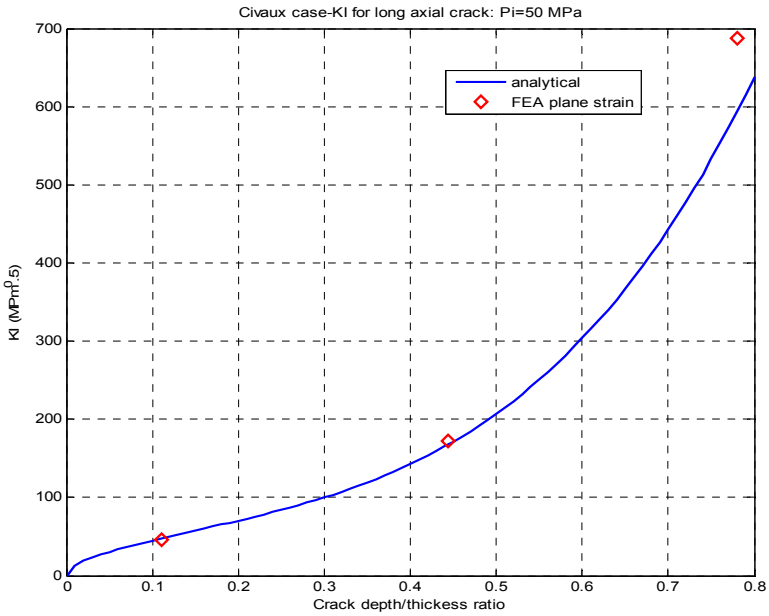

Figure A4.2 K_{Iaxial} comparison for long axial crack on inner surface of the pipe (Civaux geometry) under internal pressure Pi=50 MPa

In comparison with the FEA prediction a small difference (around 4-7%) is found over the range of crack depth/thickness ratio examined. Therefore, the benchmark confirms the accuracy of the analytical K_I value given knowledge of the stress distribution coefficients through thickness.

Appendix 5: Derivation of K_I for a long axial crack under hoop thermal stress

The dependence of the stress intensity factor solution, K_{Iaxial} on *a* is obtained from a forth order polynomial stress distribution, fitted to the analytical stress distribution (Equation 42). The following describes the methodology used for an instant of time corresponding to that at which the maximum value of hoop stress occurs at the inner surface, i.e. for $t_1 = \frac{3}{4.f_{cr}}$ and critical frequency f_{cr}=0.3 Hz (see Table 1).

Step1. The 4th order polynomial expression is fitted to the through-wall hoop stress profile at instant of time t_1 as a function of the radial coordinate, *r,* of the hollow cylinder;

Step2. The analytical expression from Step 1 is transformed into a function of normalized distance $r_{norm} = \frac{x}{l}$ (*x*= radial coordinate through the wall thickness starting at the inner surface, with *l*= wall thickness) giving the following of the hoop stress profile:

$$\sigma_z\left(\frac{x}{l}\right) = 198.1231 - 1290.841.\left(\frac{x}{l}\right) + 2372.519\left(\frac{x}{l}\right)^2 - 1808.3494\left(\frac{x}{l}\right)^3 + 510.7206\left(\frac{x}{l}\right)^4 . \quad \text{(A5.1)}$$

The shape of the stress profile described by Equation A5.1 is shown in Figure A5.1.

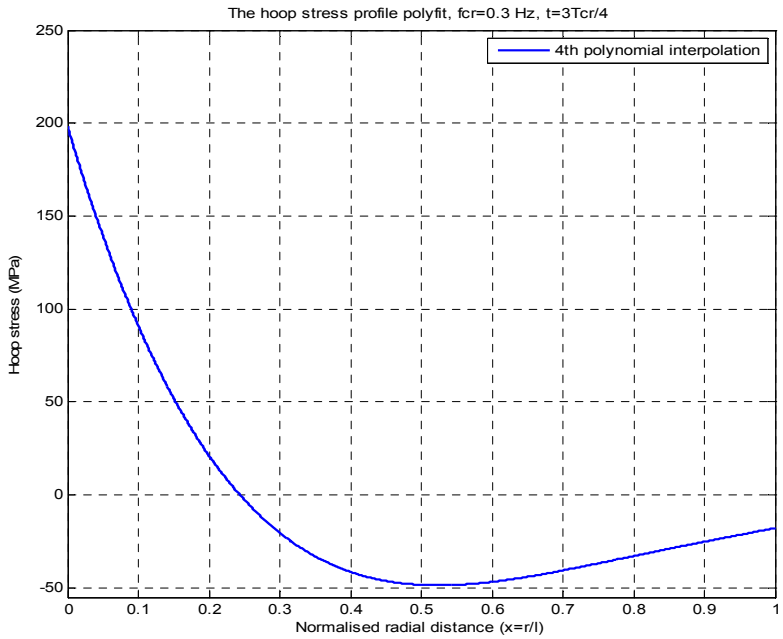

Figure A5.1. The hoop stress profile for normalized radial distance (f_{cr}=0.3 Hz, t_1=3T_{cr}/4)

Step3. The analytical expression from Equation (A5.1) allows extraction of the following polynomial coefficients by comparison with Equation (42):

$\sigma_0 = 198.1231$ MPa;

$\sigma_1 = -1290.841$ MPa;

$\sigma_2 = 2372.519$ MPa; (A5.2)

$\sigma_3 = -1808.3494$ MPa;

$\sigma_4 = 510.7206$ MPa;

Step4. Using the influence coefficients (Equation 52 to 56) and the coefficients from Equation (A5.2), the dependence of the stress intensity factor K_{Iaxial} on crack depth *a* is given by

$$K_{Iaxial}\left(\frac{a}{l}\right)=\left[\left(10.6083\cdot\left(\frac{a}{l}\right)^3-1.9273\cdot\left(\frac{a}{l}\right)^2+1.2123\cdot\left(\frac{a}{l}\right)+1.1143\right)\cdot 198.1231-\right.$$
$$\left(3.5302\cdot\left(\frac{a}{l}\right)^3-0.4091\cdot\left(\frac{a}{l}\right)^2+0.4166\cdot\left(\frac{a}{l}\right)+0.6799\right)\cdot 1290.841\cdot\left(\frac{a}{l}\right)+$$
$$\left(1.775\cdot\left(\frac{a}{l}\right)^3-0.11\cdot\left(\frac{a}{l}\right)^2+0.215\cdot\left(\frac{a}{l}\right)+0.5234\right)\cdot 2372.519\cdot\left(\frac{a}{l}\right)^2- \quad \text{(A5.3)}$$
$$\left(1.0823\cdot\left(\frac{a}{l}\right)^3-0.0284\cdot\left(\frac{a}{l}\right)^2+0.1364\cdot\left(\frac{a}{l}\right)+04397\right)\cdot 1808.3494\cdot\left(\frac{a}{l}\right)^3+$$
$$\left.\left(0.7044\cdot\left(\frac{a}{l}\right)^3+0.056\cdot\left(\frac{a}{l}\right)^2+0.0914\cdot\left(\frac{a}{l}\right)+0.3785\right)\cdot 510.7206\cdot\left(\frac{a}{l}\right)^4\right]\cdot\sqrt{\pi.a}$$

Step 5. By setting the wall thickness of the pipe as *l*=0.009 m from the Civaux 1 case, the K_{Iaxial} form depends only on crack depth *a*;

Step 6. The same steps are performed for each instant of time chosen during a thermal loading period.

Appendix 6: Derivation of K_I for fully circumferential crack under axial thermal stress

In the case of a fully circumferential crack under axial thermal stress the procedure to determine stress intensity factor $K_{Icirc}(a)$ is the same as in Appendix 5, taking into account fixed boundary conditions (ε_z=0) and critical frequency f_{cr}=0.1Hz (see Table 2). The stress intensity factor solution is obtained by using the fourth order polynomial stress distribution obtained by curve-fitting the analytical stress distribution (Equation 42) at a instant of time with the maximum value of axial stress component at inner surface(ε_z=0),i.e. for $t_1 = \frac{3}{4.f_{cr}}$.

Step1. The 4th order polynomial expression is fitted to the through-wall axial stress profile as a function of the radial;

Step2. The analytical expression from Step1 is transformed into a function of normalized distance $\frac{x}{l}$ as

$$\sigma_z\left(\frac{x}{l}\right) = 210.5979 - 608.3667.\left(\frac{x}{l}\right) + 242.1039\left(\frac{x}{l}\right)^2 + 352.8728\left(\frac{x}{l}\right)^3 - 211.9203\left(\frac{x}{l}\right)^4 . \qquad \text{(A6.1)}$$

The shape of the stress profile described by Equation A6.1 is shown in Figure A6.1.

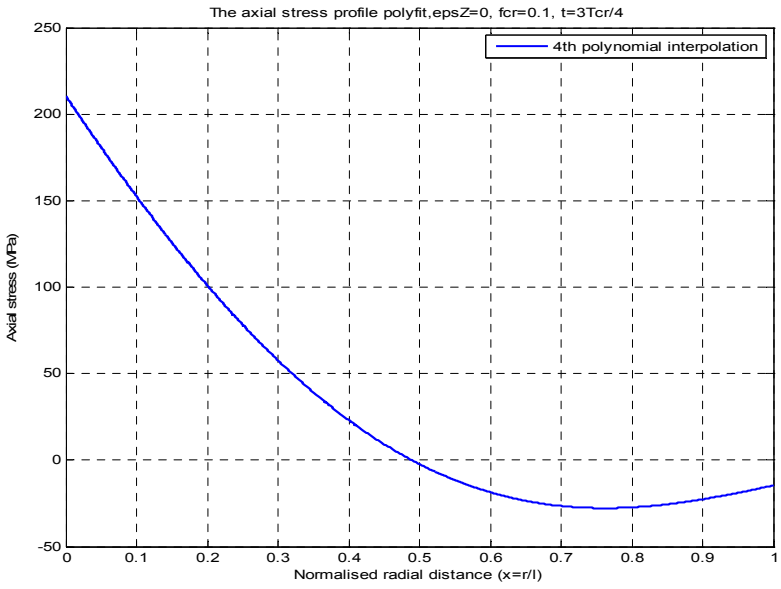

Figure A4.2. Elastic axial stress function in normalized form (f_{cr}=0.1 Hz, t_1=3T_{cr}/4)

Step3. The analytical expression in Equation (A6.1) allows extraction of the following polynomial coefficients by comparison with Equation (42):

$\sigma_0 = 210.5979$ MPa;

$$\sigma_1 = -608.3667 \text{ MPa};$$
$$\sigma_2 = 242.1039 \text{ MPa};$$
$$\sigma_3 = 352.8728 \text{ MPa};$$
$$\sigma_4 = -211.9203 \text{ MPa};$$

(A6.2)

Step4. Using the influence coefficients of axial stress distribution (Equation 58 to 62) and the coefficients from (A6.2),we obtain the dependence of the stress intensity factor K_{Icirc} on crack depth

$$K_{Icirc}\left(\frac{a}{l}\right) = \left[\left(-0.5521.\left(\frac{a}{l}\right)^3 + 2.9663.\left(\frac{a}{l}\right)^2 + 0.1938.\left(\frac{a}{l}\right) + 1.1198 \right).210.5979 - \right.$$
$$\left(0.1385.\left(\frac{a}{l}\right)^3 + 0.7604.\left(\frac{a}{l}\right)^2 + 0.1654.\left(\frac{a}{l}\right) + 0.6812 \right).608.3667.\left(\frac{a}{l}\right) +$$
$$\left(0.3354.\left(\frac{a}{l}\right)^3 + 0.1388.\left(\frac{a}{l}\right)^2 + 0.1608.\left(\frac{a}{l}\right) + 0.5234 \right).242.1039.\left(\frac{a}{l}\right)^2 +$$
$$\left(0.4271.\left(\frac{a}{l}\right)^3 - 0.1345.\left(\frac{a}{l}\right)^2 + 0.1557.\left(\frac{a}{l}\right) + 0.4391 \right).352.8728.\left(\frac{a}{l}\right)^3 -$$
$$\left. \left(0.2211.\left(\frac{a}{l}\right)^3 + 0.0151.\left(\frac{a}{l}\right)^2 + 0.0937.\left(\frac{a}{l}\right) + 0.3785 \right).211.9203.\left(\frac{a}{l}\right)^4 \right].\sqrt{\pi.a}$$

(A6.3)

Step 5. By setting the wall thickness of the pipe as *l*=0.009 m from the Civaux 1 case, the final form of K_{Icirc} depends only on crack depth*;*

Step 6. The same steps are performed for each instant of time during a thermal loading period.

European Commission

EUR 23223 EN – Joint Research Centre – Institute for Energy

Title: **Assessment of thermal fatigue crack growth in the high cycle domain under sinusoidal thermal loading** *An application – Civaux 1 case*

Author(s): V. Radu
E. Paffumi
N. Taylor
K.-F. Nilsson

Luxembourg: Office for Official Publications of the European Communities
2007 – 63 pp. – 21 x 29.7 cm
EUR – Scientific and Technical Research series – ISSN: 1018-5593
ISBN: 978-92-79-08218-4
DOI: 10.2790/4943

Abstract

The assessment of fatigue crack growth due to cyclic thermal loads arising from turbulent mixing presents significant challenges, principally due to the difficulty of establishing the actual loading spectrum. So-called sinusoidal methods represents a simplified approach in which the entire spectrum is replaced by a sine-wave variation of the temperature at the inner pipe surface. The amplitude can be conservatively estimated from the nominal temperature difference between the two flows which are mixing; however a critical frequency value must be determined numerically so as to achieve a minimum predicted life. The need for multiple calculations in this process has lead to the development of analytical solutions for thermal stresses in a pipe subject to sinusoidal thermal loading, described in a companion report.

Based on these stress distributions solutions, the present report presents a methodology for assessment of thermal fatigue crack growth life. The critical sine wave frequency is calculated for both axial and hoop stress components as the value that produces the maximum tensile stress component at the inner surface. Using these through-wall stress distributions, the corresponding stress intensity factors for a long axial crack and a fully circumferential crack are calculated for a range of crack depths using handbook *K* solutions. By substituting these in a Paris law and integrating, a conservative estimate of thermal fatigue crack growth life is obtained. The application of the method is described for the pipe geometry and loadings conditions reported for the Civaux 1 case. Additionally, finite element analyses were used to check the thermal stress profiles and the stress intensity factors derived from the analytical model. The resulting predictions of crack growth life are comparable with those reported in the literature from more detailed analyses and are lower bound, as would be expected given the conservative assumptions made in the model.

The mission of the JRC is to provide customer-driven scientific and technical support for the conception, development, implementation and monitoring of EU policies. As a service of the European Commission, the JRC functions as a reference centre of science and technology for the Union. Close to the policy-making process, it serves the common interest of the Member States, while being independent of special interests, whether private or national.

JRC
EUROPEAN COMMISSION

LD-NA-23223-EN-C

ISBN 978-92-79-08218-4

Publications Office
Publications.eu.int